In vitro and in vivo anticancer activity of tridentate thiosemicarbazone copper complexes: Unravelling an unexplored pharmacological target

In vitro and *in vivo* anticancer activity of tridentate thiosemicarbazone copper complexes: unravelling an unexplored pharmacological target

Mauro Carcelli[a], Matteo Tegoni[a], Jennifer Bartoli[a], Cristina Marzano[b], Giorgio Pelosi[a], Marika Salvalaio[b], Dominga Rogolino*[,a] and Valentina Gandin*[,b]

[a]*Dipartimento di Scienze Chimiche, della Vita e della Sostenibilità Ambientale and Consorzio Interuniversitario di Ricerca in Chimica dei Metalli nei Sistemi Biologici, Università di Parma, Parco Area delle Scienze 11/A, 43124 Parma, Italy*

[b]*Department of Pharmaceutical and Pharmacological Sciences, University of Padova via F. Marzolo 5, 35131 Padova - Italy*

ABSTRACT: Metal complexes can have a great antitumor activity, as the use of cisplatin in therapy has been demonstrating for the past fifty years. Copper complexes, in particular, have attracted much attention as an example of anticancer compounds based on an endogenous metal. In this paper we present the synthesis and the activity of a series of copper(II) complexes with variously substituted salicylaldehyde thiosemicarbazone ligands. The *in vitro* activity of both ligands and copper complexes was assessed on a panel of cell lines (HCT-15, LoVo and LoVo oxaliplatin resistant colon carcinoma, A375 melanoma, BxPC3 and PSN1 pancreatic adenocarcinoma; BCPAP thyroid carcinoma, 2008 ovarian carcinoma, HEK293 non-transformed embryonic kidney), highlighting remarkable activity of the metal complexes, in some cases in the low nanomolar range. The copper(II) complexes **1-6** were also screened, with good results, against 3D spheroids of colon (HCT-15) and pancreatic (PSN1) cancer cells. Detailed investigations on the mechanism of action of the copper(II) complexes are also reported: they are able to potently inhibit Protein Disulfide Isomerase, a copper-binding protein, that is recently emerging as a new therapeutic target for cancer treatment. Good preliminary results obtained in *in vivo* tests indicate that this series of metal-based compounds could be a very promising weapon in the fight against cancer.

Keywords: thiosemicarbazones; copper complexes; anticancer compounds; Protein Disulfide Isomerase inhibitors; nanomolar activity; X-ray structure

1. INTRODUCTION

Bioinorganic chemistry can offer an innovative approach to many issues in the biomedical arena, allowing to exploit the characteristics of metal ions (redox activity, interaction with cellular proteins, alteration of homeostatic equilibria) in synergy with organic ligands [1,2]. The cisplatin milestone is an epitome in this field. It is in fact one of the most used anticancer agents in several therapeutic regimens, in combination with other drugs, including topoisomerase II inhibitors (like doxorubicin or bleomycin), antimetabolites (e.g. gentamicin, 5-fluorouracil, methotrexate), and taxol [3,4]. However, its strong activity is accompanied by a poor selectivity, with consequent important side effects such as neurotoxicity, nephrotoxicity and ototoxicity, that limit its efficacy. In addition, the use of cisplatin can be undermined by innate or acquired drug resistance[5,6]. Therefore, extensive research is on-going in order to develop other metal-based anti-tumor compounds with improved pharmacological profiles. Researchers have been extensively investigating the possibility of using endogenous metals, since they could be less toxic and more selective than platinum[7].

In this scenario, copper has attracted considerable interest, also due to the different response of tumor cells to the presence of this metal when compared to healthy ones. It has been verified that in cancerous tissues the concentration of Cu^{2+} is much higher than that found in healthy tissues [8,9,10]. This fact has been related to the crucial role of copper in the angiogenesis processes and, consequently, in tumor growth and metastasis formation [11]. The “tumor-specific” high copper level could represent a key target to develop novel selective anticancer drugs. Two different approaches [12] have been pursued so far: the use of chelating compounds able to sequester copper ions and the development of copper(I/II)-based antitumor drugs. If, schematically, the mode of action of cisplatin is ascribable to its ability to crosslink the purine bases of DNA, causing DNA damages, and subsequently inducing apoptosis in cancer cells, the questions about the mechanism of action of anticancer copper complexes are mainly still unanswered [12,13,14].

The role of the ligands in the activity of the metal complexes is obviously crucial, since they can modulate important aspects such as lipophilicity, solubility, stability versus sequestration by serum or cellular proteins. A very interesting class of ligands studied so far for their anticancer activity is constituted by thiosemicarbazones (TSCs) [15,16,17]. The most outstanding representative of this class of compounds is Triapine (3-AP, **Fig. 1**), that has already entered a number of clinical trials [18,19]. Moreover, very recently, other promising TSCs, like di-2-pyridylketone 4-cyclohexyl-4-methyl-3-thiosemicarbazone (DpC) and (E)-N′-(6,7-dihydroquinolin-8(5H)-ylidene)-4-(pyridin-2-yl)piperazine-1-carbothiohydrazide (COTI-2) (**Fig. 1**), have also entered clinical trials [20,21].

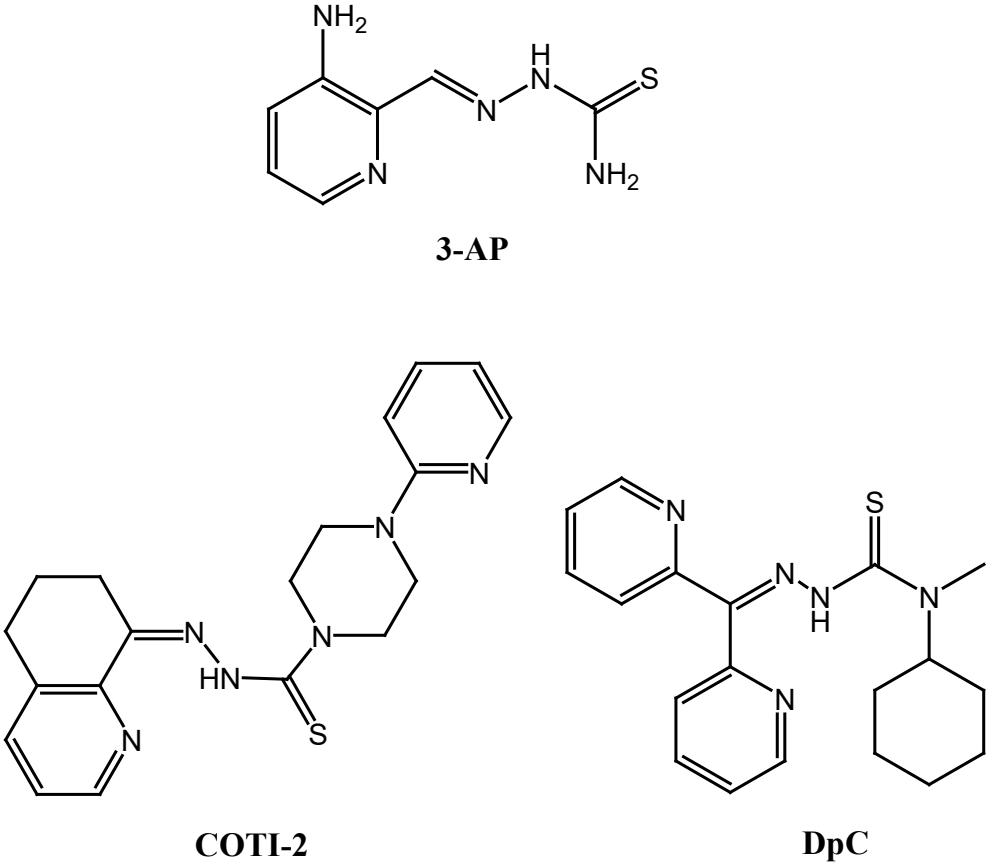

Fig. 1. Schematic representation of thiosemicarbazones in clinical trial.

TSCs represent a very diversified class, in which structural variations can have different mechanisms of action and modulate different pathways, also as a function of their coordinating properties, since the role of metal chelation seems to be crucial in relation to their anticancer activity [22,23,24]. TSCs

can form a great variety of coordination compounds with biologically-relevant transition metal ions, like iron(II/III), copper (I/II) and zinc(II) [16,25,26]. Interestingly, metal complexes very often show enhanced cytotoxic profiles and alternative modes of action when compared with the parent ligands. Many investigations highlighted the ability of TSCs metal complexes to inhibit enzymatic pathways related to DNA synthesis and polymerization (i.e. to inhibit ribonucleotide reductase or DNA polymerase) [27,28,29]. TSCs can also chelate intracellular iron and consequently establish redox cycling of the Fe(TSC) complexes to produce oxygen reactive species (ROS) within the cytoplasm [15,30,31]. The chelation properties of TSCs can be exploited also to target copper(II) and its homeostasis [12,32]. Copper, as well as iron, can be involved in the Haber-Weiss reaction and in the production of ROS, the activation of redox cycles and the reduction of GSH, inducing oxidative stress [12,33]; in addition, other pathways are probably also to be taken into account [12,34,35].

With these considerations in mind and looking at encouraging previous results that we obtained with salicylaldehyde-TSCs [36,37,38], we focused our attention on the 2,3-dihydroxy- and 2-hydroxy-3-methoxy-benzaldehyde thiosemicarbazone derivatives **HL^1-HL^6**, with different substituents at the N4 nitrogen (**Fig. 2**). Salicylaldehyde thiosemicarbazones behave essentially as tridentate ligands, but they can also be involved in the formation of polynuclear species [39]. The copper(II) complexes **1-6** (**Fig. 2**) with **HL^1-HL^6** were characterized in solution by means of UV-visible spectrophotometric titrations, and in the solid state, also by means of X-ray diffraction analysis. The antitumor properties of **HL^1-HL^6** and **1-6** were assayed *in vitro* on a panel of cell lines (HCT-15, LoVo and LoVo oxaliplatin resistant colon carcinoma, A375 melanoma, BxPC3 and PSN1 pancreatic adenocarcinoma, BCPAP thyroid carcinoma, 2008 ovarian carcinoma, HEK293 non-transformed embryonic kidney). The *in vivo* antitumor activity of **1**, the most promising copper(II) complex, was finally evaluated. Detailed investigations on the mechanism of action of the copper(II) complexes **1-6** are also reported, unveiling new possible biological targets so far unexplored.

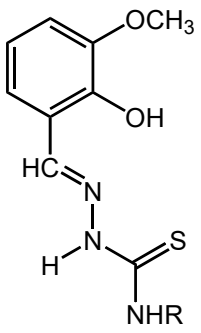

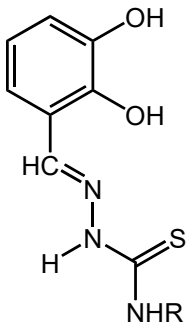

R = H **HL[1]**
Ph **HL[2]**
Et **HL[3]**

R = H **HL[4]**
Ph **HL[5]**
Et **HL[6]**

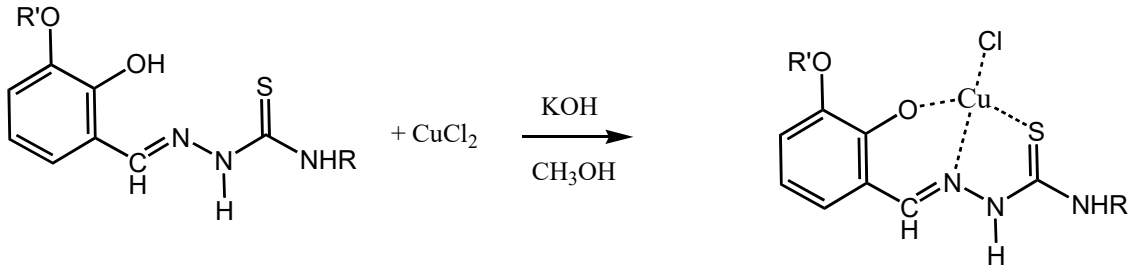

R \ R'	OCH_3	OH
H	**1**	**4**
Ph	**2**	**5**
Et	**3**	**6**

1-6

Fig. 2. The ligands **HL[1]-HL[6]** and the corresponding copper(II) complexes **1-6**.

2. RESULTS AND DISCUSSION

2.1 Synthesis. The thiosemicarbazone ligands **HL[1]-HL[6]** (**Fig. 2**) were synthesized in high yields by condensation of thiosemicarbazide or 4-*N*-substituted-3-thiosemicarbazide with 2-hydroxy-3-methoxybenzaldehyde or 2,3-dihydroxybenzaldehyde. They were satisfactorily characterized by usual spectroscopic and spectrometric techniques and experimental data are in accordance with the literature data [36,57]. The ligands are in the *E* form in solution, as evidenced by the chemical shift values of the HC=N and NH protons in the ^{1}H-NMR spectrum in DMSO-d_6 [57]. **HL[1]-HL[6]** can give

rise to thione-thiol tautomerism, but the absence, in the IR spectrum, of the S–H stretching band near 2600 cm^{-1} and the presence of a N–H stretching band in the range 3130-3170 cm^{-1} are indicative of the presence of the thione form [40,12].

HL^1-HL^6 are versatile ligands: they can coordinate to transition metal ions *via* the *O, N* and *S* donor atoms, acting as bidentate or tridentate. Some examples are reported in the literature of copper(II) complexes with salicylaldehyde TSCs, with different stoichiometry and coordination geometry depending on the experimental conditions used [41,39]. The metal complexes **1-6** (**Fig. 2**) were obtained by reacting $CuCl_2$ with the ligands in methanol, and adjusting the pH to 8-9 with NaOH in order to force the deprotonation of the ligand. To avoid possible oxidative cyclization reactions [42], synthesis were carried out under nitrogen by using degassed solvents. In the IR spectra of **1-6**, the iminic bond stretching vibrations, assigned to bands around 1522-1608 cm^{-1} in the ligands, underwent up-shifts of 15-60 cm^{-1} upon complexation, indicating the involvement of this group in coordination. Elemental analysis suggested the isolation of complexes of general formula $[CuLCl]\cdot nH_2O$, with a 1:1 metal to ligand *ratio*, and various grades of hydration. In the ESI mass spectra of **1-6**, recorded in methanol in positive ion mode, there are the peaks relative to the species $[CuL]^+$, corresponding to the loss of a chloride ion.

Overall, the data suggested the formation of a 1:1 metal chelate for all the complexes **1-6**, with the mono-deprotonated ligand behaving as *O,N,S* tridentate, and a chloride ion completing the coordination sphere of the Cu(II) ion (**Fig. 2)**.

2.2 X-ray discussion. The crystal structure of $[CuL^1Cl]\cdot H_2O$ had already been reported [43],but since it was collected at 123K, we have decided to recollect the data at room temperature to see if there are significant structural differences. The structure is obviously substantially the same, but we reached a better R value and noticed a few details which are worth to be reported. The geometry around the copper atom (**Fig. 3**) is in both structures slightly distorted from the ideal square planar with the bond angles ranging between 86.30(8) and 92.39(7) [86.54(8) and 92.23(6)] (in square parentheses the values reported in Sen's paper). The coordination distances remain very similar: Cu–S 2.263(1)Å

[2.262(9)Å, this distance reported in Sen's description is actually wrong being 2.662Å], Cu–N 1.952(3)Å [1.951(2)Å], Cu–O 1.919(2)Å [1.918(2)Å], and Cu–Cl 2.259(1)Å [2.266(1)Å].

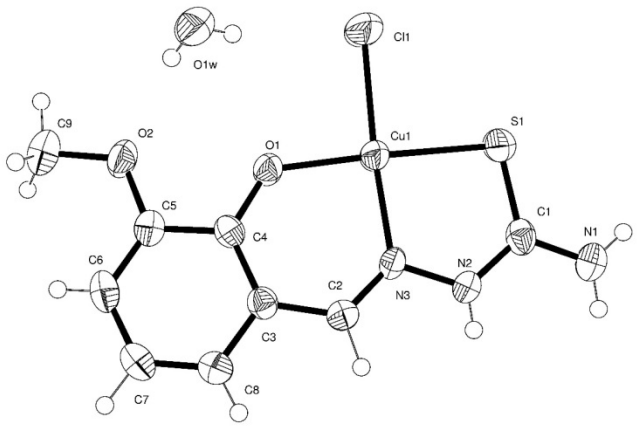

Fig. 3. ORTEP plot of the crystal structure of $[CuL^1Cl]\cdot H_2O$ (probability 50%).

Noteworthy is that, at room temperature, the C=S bond is shorter (1.697(4) Å) than at lower temperature, 1.708(3) Å, and that the ligand is more twisted, with an angle between the average plane of the aromatic ring and that of the TSC fragment of 4.70° (4.58° at low temperature).

The crystal structure of $\{Na[CuL^3Cl]_2Cl\}$ is characterized by the presence of a sodium ion that plays a key role in the packing by coordinating the oxygen and the chlorine atoms of two $[CuL^3Cl]$ units (**Fig. 4**).

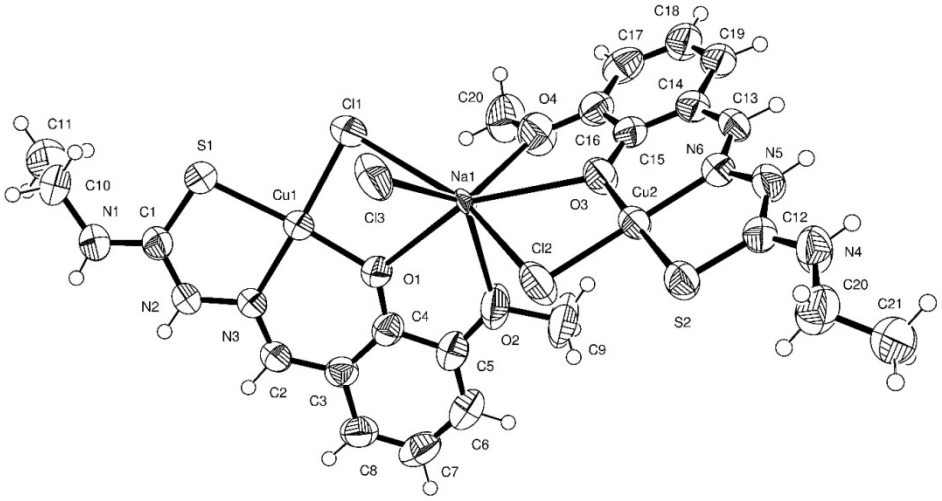

Fig. 4. ORTEP plot of the crystal structure of {Na[CuL^{3}Cl]$_2$Cl} (probability 50%).

The two units taken singularly present structures very similar to the one reported above for [CuL^{1}Cl]·H$_2$O. Apart from the presence of the ethyl fragment on the TSC terminal amino group, the rest of the molecule presents approximately the same geometrical parameters. The sodium ion is surrounded by four oxygens belonging to the ligands, two chlorine atoms that are coordinated by the copper and a third chloride which acts as a counterion to neutralize the sodium positive charge.

Bond distances (Å) and angles (°) for [CuL^{1}Cl]·H$_2$O and {Na[CuL^{3}Cl]$_2$Cl}are reported in **Table S1** and **Table S2**, respectively.

2.3 Studies in solution. We have studied the complexes formed by Cu(II) ions with the ligands **HL^1** and **HL^4** in solution by means of spectrophotometric techniques. The study of the complexation equilibria for the system Cu(II)/**HL^1** required the use of a competitive Zn(II)/Cu(II) titration strategy; for these reasons, the stability of the complexes with Zn(II) was also examined.

All the metal:ligand systems were investigated by means of spectrophotometric titrations of the ligand solutions with the metal ions. Since the data are collected in HEPES buffer at pH 7.4, the determined formation constants are *conditional*, *i.e.* their values reflect the stability of the complexes species under these specific medium conditions. The possible competing role of HEPES toward the

complexation of Cu(II) on the basis of the reported stability constants was taken into account [44]. As for Zn(II), data are reported in the literature about such competing equilibria [45], but they have been considered questionable [46]. On the basis of the Irving-Williams series we expect that the stability of Zn(II) complexes with HEPES are lower than those of Cu(II), therefore negligible in our case. Perhaps more important, we should also note that the buffered conditions did not allow to establish the protonation state of the ligands in solution (either free or coordinated). Therefore, hereafter, in the study of the complexation equilibria, the free and complexed forms of the ligands will be reported as $\mathbf{L^1}$ or $\mathbf{L^4}$, where L represents the ensemble of the ligands in all their different protonation states and charges are omitted.

The ligands have strong absorption bands at *ca*. 300-325 nm (ε *ca*. 32000 M^{-1} cm^{-1} for $\mathbf{HL^1}$, 19000 M^{-1} cm^{-1} for $\mathbf{HL^4}$, see **Fig. S7** and **S18**, Supporting information). As a general behavior, upon addition of the metal ions, a band at *ca*. 370-400 nm appeared in all titrations. This band, associated to the formation of complex species, is due to intra-ligand or, for copper(II), to ligand to metal charge transitions. At these dilution levels (*ca*. 40 μM), ligand-field transitions for the Cu(II) species are not expected to be observable. UV visible spectra, titration curves and Job's plots for the studied systems are reported in **Fig. S7-S22**.

We first examined the system Cu(II)/$\mathbf{HL^1}$. This ligand forms the 1:1 Cu(II):ligand species that has been characterized in the solid state and is expected to be present also in solution in significant amount. Actually, the spectral dataset for the titration of $\mathbf{HL^1}$ with Cu(II) presents two bands, one at *ca*. 320 nm and one at *ca*. 390 nm which decrease and increase respectively upon addition of the titrant (**Fig. 5**).

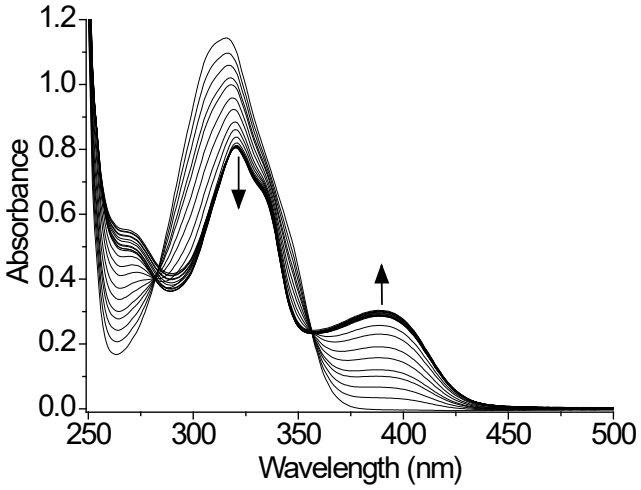

Fig. 5. UV-visible spectra for the titration of **HL^1** with Cu(II) in methanol:water 9:1 (*v/v*) at pH 7.4 (25 mM HEPES buffer. C_{L1} = 41 μM, **HL^1**:Cu(II) = 1:0-2.1).

The evaluation of the absorbance values at 388 nm (**Fig. S8**) and the Job's plot (**Fig. S9**) strongly suggests the formation of a predominant Cu(II)/ligand 1:1 species. Unfortunately, the titration endpoint (**Fig. S8**) is very pronounced and this situation prevents the determination of the formation constant.

We decided therefore to adopt a strategy which involves the use of Zn(II) as competing metal ion for the complexation of **HL^1**. Through this strategy, it is possible to study equilibria of the form ZnL + Cu = CuL + Zn, and to determine the formation constants of the Cu(II) species, given the formation constants of the Zn(II) ones. Firstly, we carried out the titration of **HL^1** with Zn(II): the spectral dataset (**Fig. S10**) shows a behavior similar to that observed with Cu(II). The results of the data treatment suggested the formation of a [Zn(**L^1**)] species, in agreement with the Job's plot data (**Fig. S12**). The formation constant is reported in **Table 1**. Lastly, we carried out the titration with Cu(II) of a solution containing **HL^1** and Zn(II) in 1:2 ratio. The spectral dataset (**Fig. S14**) is consistent with the interconversion of one predominant species ([Zn(**L^1**)]) into a secondo one ([Cu(**L^1**)]). This hypothesis is supported by the decrease of a band at *ca*. 375 nm (Zn(II) complex) with increase at *ca*. 390 nm (Cu(II) species). We have treated this spectral dataset by using the formation constant and

the molar spectrum of the [Zn($\mathbf{L^1}$)] species as fixed parameters, along with the molar spectrum of $\mathbf{HL^1}$. The best fitting of the experimental data was indeed obtained with a [Cu($\mathbf{L^1}$)] species, leading to the calculation of the formation constant reported in **Table 1**.

The spectra dataset for the titration of $\mathbf{HL^4}$ with Cu(II) (**Fig. 6**) was more complicated compared to that of $\mathbf{HL^1}$, and it suggests the formation of more than one complex species.

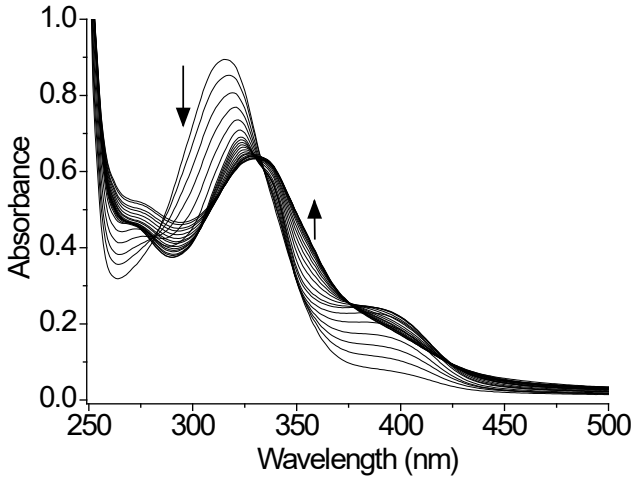

Figu. 6. UV-visible spectra for the titration of $\mathbf{HL^4}$ with Cu(II) in methanol:water 9:1 (*v/v*) at pH 7.4 (25 mM HEPES buffer. C_{L4} = 41 μM, $\mathbf{HL^4}$:Cu(II) = 1:0-2.6).

Actually, for the addition of the first equivalent of Cu(II), the band at 310 nm decreases in intensity, with concomitant increase of the band at 390 nm. This behavior is similar to that observed for the titration of $\mathbf{HL^1}$, and was provisionally associated to the formation of a predominant [Cu($\mathbf{L^4}$)] complex. Upon addition of a second equivalent of Cu(II), the band at 390 nm decreases with increase of the shoulder at *ca*. 355-360 nm, and the consequent appearance of an isosbestic point at 374 nm. No further significant changes in the spectra occurred after the addition of 2 equivalents of Cu(II). The formation of two predominant species seems plausible: a Cu(II):ligand 1:1 species for the addition of the first equivalent of copper(II), and a 2:1 Cu(II):ligand species upon addition of the second equivalent of metal. We then treated the entire dataset, obtaining the best fitting of the experimental data by considering three species: two mononuclear ([Cu($\mathbf{L^4}$)] and [Cu($\mathbf{L^4}$)$_2$]) species,

and a bimetallic ([Cu_2(**L^4**)]) one (**Figure S16**); their formation constants are reported in **Table 1**. Remarkably, the bimetallic species has been found for **HL^4** but not for **HL^1**: the 2,3-dihydroxyphenyl group in **HL^4** may act as another binding site for Cu(II), with consequent formation of a bimetallic complex in excess of metal. For the sake of completeness, we have also studied the Zn(II)/**HL^4** system (**Fig. S19**). In the treatment of these spectral data we have considered the species [Zn(**L^4**)] and [Zn(**L^4**)$_2$], as suggested by the Job's plot at 376 nm, which has its maximum for $\chi > 0.5$ (**Fig. S21**). The stability constants of these Zn(II) species are reported in **Table 1**.

Table 1. Logarithms of the conditional formation constants of the Cu(II) and Zn(II) complexes with **HL^1** and **HL^4** in HEPES buffer (25 mM, pH 7.4) in methanol:water 9:1 (*v/v*), at 298.2 K. Charges are omitted for clarity. Standard deviations are reported in parentheses.

	HL^1	**HL^4**
[Cu(L)]	7.90(3)	7.32(18)
[Cu(L)$_2$]	-	13.0(2)
[Cu_2(L)]	-	12.80(2)
[Zn(L)]	5.97(2)	6.91(11)
[Zn(L)$_2$]	-	12.0(2)

2.4 Effects on cell viability. The copper(II) thiosemicarbazone complexes **1**-**6** as well as the corresponding ligands **HL^1**-**HL^4** were tested for their cytotoxic activity by means of the MTT assay, as reported in the Experimental section. The in-house human cancer cell line panel contains examples of ovarian (2008), colon (HCT-15), pancreatic (PSN-1 and BxPC3), and thyroid (BCPAP) cancers as well as of melanoma (A375). Cisplatin was used as reference compound and was tested under the same experimental conditions. The cytotoxicity parameters, in terms of IC_{50} obtained after 72 h of exposure, are listed in **Table 2**.

Table 2. Cytotoxicity assays. Cells ($3\text{-}8\times10^3\cdot mL^{-1}$) were treated for 72 h with increasing concentrations of the tested compounds. Cytotoxicity was assessed by MTT test. IC_{50} values were calculated by 4-PL model ($P < 0.05$). S.D.= standard deviation. ND = non detectable.

	IC_{50} (μM) ± S.D.					
	2008	**HCT-15**	**PSN-1**	**A375**	**BxPC3**	**BCPAP**
HL1	0.78±0.21	0.51±0.14	0.51±0.12	0.10±0.030	0.005±0.001	0.51±0.09
1	0.013±0.008	0.004±0.001	0.008±0.002	0.003±0.0004	0.03±0.01	0.033±0.01
HL2	4.85±1.12	3.97±0.38	6.82±1.08	2.11±0.4	0.98±0.25	3.15±0.62
2	0.035±0.011	0.017±0.006	0.32±0.10	0.009±0.001	0.002±0.0005	0.84±0.16
HL3	1.97±0.66	2.22±0.76	3.13±1.11	2.23±0.78	1.11±0.76	0.51±0.090
3	0.010±0.001	0.036±0.012	0.021±0.090	0.019±0.004	0.015±0.006	0.041±0.011
HL4	ND	ND	ND	ND	ND	ND
4	0.098±0.004	0.091±0.06	0.36±0.010	0.029±0.006	0.011±0.004	0.35±0.09
HL5	ND	ND	ND	ND	ND	ND
5	0.71±0.15	0.82±0.14	0.51±0.12	0.28±0.09	0.11±0.09	0.83±0.11
HL6	ND	ND	ND	ND	ND	ND
6	0.16±0.04	0.23±0.09	0.029±0.008	0.069±0.020	0.029±0.011	0.072±0.012
CDDP	2.17 ± 1.37	13.92±1.68	12.10±2.87	3.11±0.98	13.98±1.23	6.65±2.85

TSCs **HL^1-HL^3** showed IC_{50} values in the low-micromolar range, whereas with **HL^4-HL^6** non-reproducible and non-reliable MTT results were obtained, thus precluding the calculation of these IC_{50} values. This behavior could be tentatively attributed to the scarce solubility of **HL^4-HL^6** in physiological conditions. On the other hand, copper(II) **1-6** compounds showed a significant *in vitro* antitumor activity, with IC_{50} values even in the nanomolar range.

As a general consideration, copper(II) complexes **1-3**, with the 2-hydroxy-3-methoxyphenyl group, were, on average, more cytotoxic than **4-6,** the corresponding copper(II) complexes with the 2,3-dihydroxyphenyl group. As an example, the 2-hydroxy-3-methoxybenzaldehyde thiosemicarbazone

Cu(II) complex **3** elicited average IC_{50} values over the six employed cancer cell lines of roughly 0.024 μM, compared with average IC_{50} of 0.098 μM obtained with the corresponding 2,3-dihydroxybenzaldehyde thiosemicarbazone complex **6**.

More importantly, all the tested copper(II) complexes **1-6** were significantly more cytotoxic than the reference compound cisplatin, being their IC_{50} values up to three order of magnitude lower than those calculated with the reference metal-based drug. Among all, **1** emerged as the most cytotoxic derivative with mean IC_{50} values against all tested cancer cell lines about 580 times lower than those calculated for cisplatin (average IC_{50} values of 0.015 and 8.7 μM, respectively). In particular, against human pancreatic (BxPC3 and PSN1) and colon (HCT-15) cancer cells, the copper(II) complex **1** was about 466, 1510 and 3480 times more effective than cisplatin, respectively.

Compound **5** was, on the contrary, the one endowed with the weakest *in vitro* antiproliferative effect, with average IC_{50} values over the six cancer cell lines of 0.54 μM. However, its cytotoxic activity was significantly superior (16 times) than cisplatin.

The *in vitro* antitumor activity of the complexes **1-6** was evaluated on a human colon cancer cell line pair (LoVo/LoVo-OXP) which was selected for sensitivity/resistance to oxaliplatin, the key drug in FOLFOX (folinic acid, 5-fluorouracil, and oxaliplatin) chemotherapeutic regimen for the management of colorectal cancers [47]. Similarly to cisplatin, the clinical efficacy of oxaliplatin is seriously limited by the development of cancer cell resistance and, presently, no other drugs in advanced clinical development for the treatment of patients with oxaliplatin-refractory colorectal cancer are available. Cytotoxicity on sensitive and resistant cells was assessed after 72 h of drug treatment by MTT test. **Table 3** shows the cytotoxicity parameters, in terms of IC_{50} and resistance factor (RF), the latter defined as the ratio between IC_{50} values calculated for resistant cells and those obtained with sensitive ones.

Table 3. Cross-resistance profiles. Cells ($3\times10^3\cdot mL^{-1}$) were treated for 72 h with increasing concentrations of the tested compounds. Cytotoxicity was assessed by MTT test. IC_{50} values were calculated by 4-PL model ($P < 0.05$). RF = IC_{50} resistant/IC_{50} parental cell lines. S.D.= standard deviation.

	IC_{50} (μM) ± S.D.		
	LoVo	**LoVo-OXP**	**RF**
1	0.031±0.001	0.004±0.001	0.13
2	0.029±0.008	0.030±0.010	1.03
3	0.036±0.009	0.008±0.002	0.22
4	0.020±0.001	0.020±0.001	1
5	0.21±0.08	0.09±0.01	0.43
6	0.030±0.001	0.02±0.01	0.67
oxaliplatin	2.17 ± 1.37	13.92±1.68	6.41

All copper(II) complexes exhibited activity levels very similar on both oxaliplatin-sensitive (LoVo) and -resistant (LoVo-OXP) cell lines. Actually, the RFs were from 6- to 50-fold lower than that of oxaliplatin, indicating the absence of cross-resistance phenomena.

As one of the main drawbacks of chemotherapeutic drugs are the possible toxic effects toward non-cancerous cells, we measured the cytotoxicity of **1-6** against non-cancerous cells (HEK293) and calculated the selectivity index (SI, defined as the *ratio* of the IC_{50}s in non-cancerous cells to those in cancer cells). The cytotoxicity data for HEK293 cells and the selectivity indices are reported in **Table 4**. It is worthy of note that the copper(II) complexes **2** and **3** were less cytotoxic against HEK293 non-cancerous cells, eliciting SI values even better than that calculated with cisplatin, thus indicating a preferential cytotoxicity against tumor cells. On the contrary, for complexes **1** and **4-6** the SI values clearly suggest the absence of a preferential activity against cancer cells.

Table 4. Cytotoxicity in HEK293 human non-cancerous cells. Cells (5×10^3 mL^{-1}) were treated for 72 h with increasing concentrations of tested compounds. The cytotoxicity was assessed by the MTT test. IC_{50} values were calculated by a four parameter logistic model ($P < 0.05$). S.D. = standard deviation. Selectivity index (SI) is defined as IC_{50} non-tumor/tumor cell lines (LoVo).

	IC_{50} (μM) ± S.D.	
	HEK293	**SI**
1	0.009±0.002	0.3
2	0.093±0.011	3.2
3	0.11±0.080	3.05
4	0.007±0.001	0.3
5	0.021±0.010	0.1
6	0.034±0.001	1.1
CDDP	24.38±3.45	2.1

The copper(II) compounds **1-6** were also screened against 3D spheroids of colon (HCT-15) and pancreatic (PSN1) cancer cells. 3D cell cultures, comprising cancer cells in various cell growth stages, possess several features that more closely mimic the heterogeneity and complexity of *in vivo* tumors, being potentially more predictive for *in vivo* results than conventional 2D cell cultures [48]. The cancer spheroids were treated with copper(II) complexes or cisplatin for 72 h and the cell viability was assessed by means of the acid phosphatase (APH) assay (**Table 5**). **1-6** were extremely effective, being roughly up to 60 times more active than cisplatin against HCT-15 and PSN1 cells. These latter data, attesting the ability of TSCc copper(II) complexes to penetrate in the core area of spheroids, strongly confirm the antitumor potential of these copper(II) complexes.

Table 5. Activity in 3D cell cultures. Spheroids (2.5×10^3 cells/well) were treated for 72 h with increasing concentrations of the tested compounds. The growth inhibitory effect was evaluated by means of APH test. IC_{50} values were calculated from the dose-survival curves by 4-PL model ($P < 0.05$). S.D. = standard deviation.

	IC_{50} (μM)± S.D.	
	HCT-15	**PSN-1**
1	1.08±0.38	0.90±0.02
2	3.56±1.67	1.17±0.11
3	1.25±0.98	0.90±0.3
4	1.17±0.62	0.94±0.27
5	1.69±0.45	1.18±0.23
6	1.28±0.62	0.91±0.01
CDDP	68.2±4.57	52.6±3.78

2.5 Cellular uptake and distribution. In the attempt to correlate cytotoxicity potency with the ability of the tested complexes to enter cancer cells and to distribute into cell compartments, we performed cellular uptake and distribution studies in LoVo human colon cancer cells (**Fig. 7A** and **B**). The results expressed as ppb of Cu per 10^6 cells are summarized in **Fig. 7**.

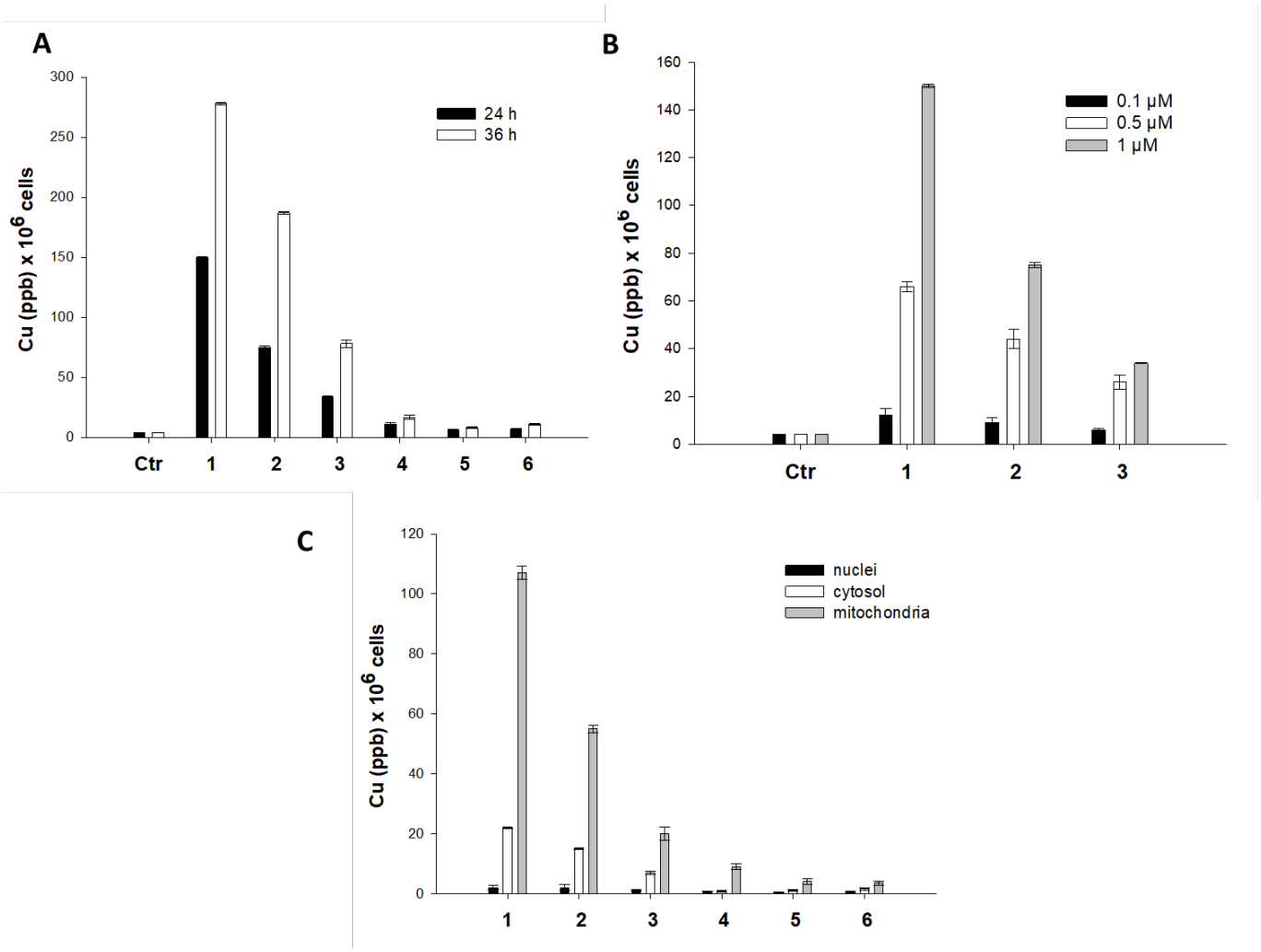

Fig. 7. Cellular uptake (A, B) and distribution studies (C) in cancer cells. (A) LoVo cancer cells were incubated with 1 µM of copper complexes for 24 or 36 h, and cellular copper content was detected by GF-AAS analysis. (B) LoVo cancer cells were incubated with 0.1, 0.5 or 1 µM of copper complexes for 24 h, and cellular copper content was detected by GF-AAS analysis. (C) LoVo cancer cells were incubated with 1 µM of copper complexes for 24 h and samples were processed for sub-fractions preparation as reported in the Experimental Section. The sub-fraction copper content was detected by GF-AAS analysis. Error bars indicate the standard deviation.

Copper(II) complexes **1-3** derived from 2-hydroxy-3-methoxybenzaldehyde thiosemicarbazones were able to accumulate in a time- and dose-dependent manner, and significantly greater with respect to the corresponding copper(II) complexes with 2,3-dihydroxybenzaldehyde thiosemicarbazones **4-6**, which poorly permeated cancer cells, independently of exposure time (**Fig. 7**, **A** and **B**). The 2-hydroxy-3-methoxybenzaldehyde derivative **1** was the most effective in entering cancer cells; after 24 or 36 h, in **1**-treated an intracellular copper content roughly 10 times higher than in **4**-**6**-treated cells was detected. However, by comparing uptake and cytotoxicity data in LoVo human colon cancer cells, a direct correlation between cellular accumulation and cytotoxic potency does not result.

Concerning cellular content, nuclear and mitochondrial levels of copper(II) complexes in LoVo cancer cells, it is evident that 2-hydroxy-3-methoxyphenyl compounds **1-3** accumulated substantially in the mitochondria fraction and, to a lesser extent, in cytosolic fractions (**Fig. 7 C**). Conversely, very low levels of copper were found in the nuclei of treated cancer cells. A similar cellular distribution was found for 2,3-dihydroxyphenyl copper(II) compounds **4-6**, but detected copper amounts were about one order of magnitude lower.

Mechanistic studies. Since the '60s copper has been found to possess high DNA binding affinity, depending on copper complex size, electron affinity, and geometry of the formed adduct. DNA has been referenced as the main molecular target for various copper(II) complexes in many studies [12]. On this basis, we thought of interest to evaluate the ability of copper(II) complexes **1-6** to damage DNA. LoVo cancer cells were treated with **1-6** for 6 and 12 h, and DNA fragmentation was estimated by using the alkaline single cell gel electrophoresis (comet assay). The results were compared with those obtained after treatment of LoVo cells with equitoxic concentrations of dichloro(1,10-phenanthroline)copper(II) (Cu(phen)) a well-known copper complex with nuclease activity (**Fig. 8 A** and **B)**. LoVo cancer cells treated with **1-6** showed no increase in electrophoretic migration of DNA fragments, and comet tail lengths of analyzed single cells were below 1 μm. On the contrary, Cu(phen)-treated LoVo cells displayed a statistically significant increase in DNA fragmentation.

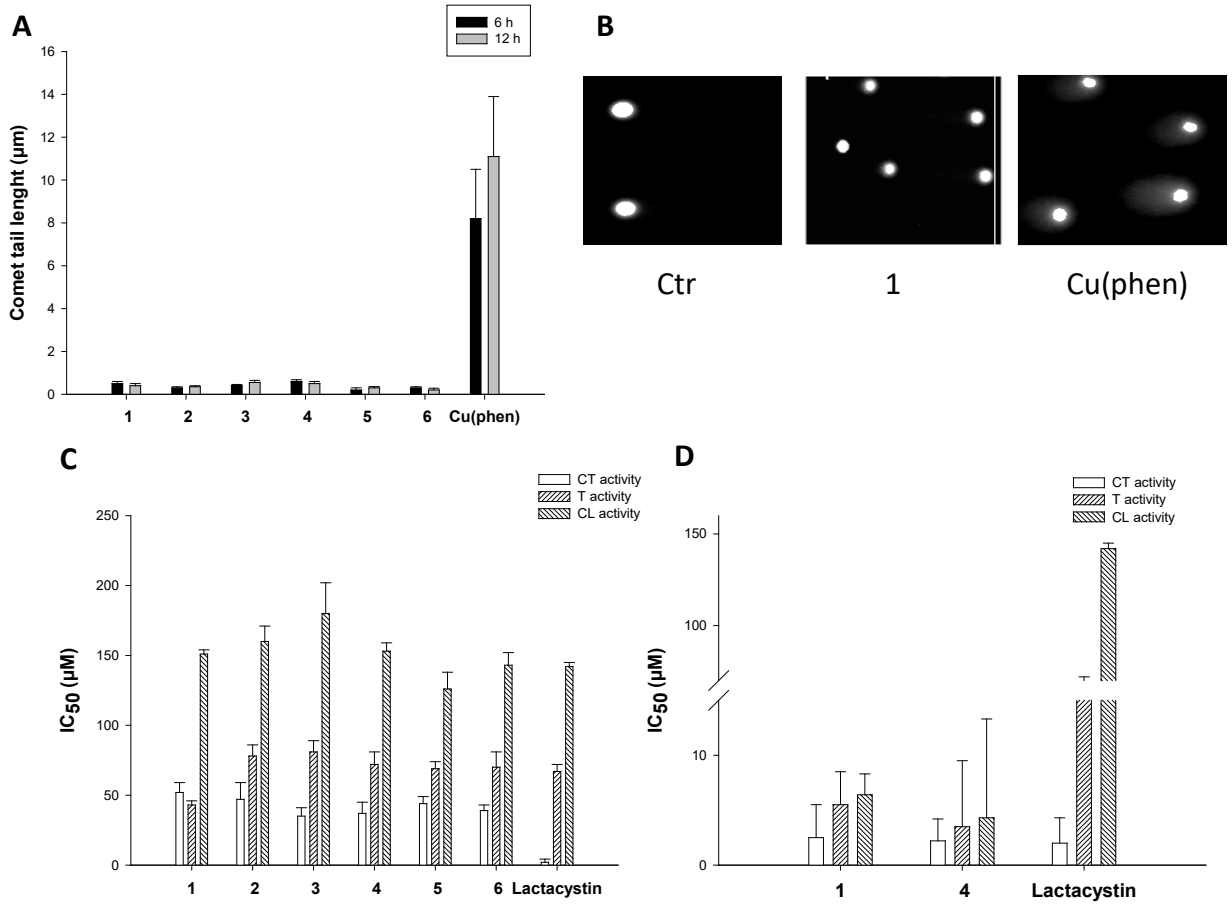

Fig. 8. Mechanistic studies: DNA damage (A and B) and proteasome inhibition (C and D). (A) LoVo cells were treated for different incubation times (6 or 12 h) with 1 µM of the tested complexes and then processed for comet assay as reported in the Experimental Section. Comet tail length was calculated from the center of the cell and measured in micrometers with CellF software. The error bars indicate the standard deviation. (B) Representative images of LoVo cells after 12 h incubation with compound **1** or Cu(phen). (C) Inhibition of CT-L, T-L and C-L activities of purified rabbit 26S proteasome after 60 min of incubation with increasing concentrations of compounds **1-6** or Lactacystin. Proteasome catalytic activity was estimated by means of specific fluorogenic substrates. IC_{50} values were calculated by 4-PL model ($P < 0.05$). The error bars indicate the standard deviation. (D) LoVo cells were treated for 24 h with increasing concentrations of complexes **1** and **4**. Proteasome catalytic activities were estimated fluorometrically as reported in C. The error bars indicate the standard deviation.

It has been previously demonstrated that some metal-based compounds exert their antiproliferative activity by inhibiting the proteolytic proteasome activities. In particular, various classes of copper complexes were reported to behave as proteasome inhibitors [12, 49]. On these bases, the ability of **1-6** to hamper the functioning of chymotriptic-like (CT-L) activity was first assessed *in vitro*, on purified rabbit 26S proteasome after incubation with increasing concentrations of the tested compounds or Lactacystin, an irreversible nonpeptidomimetic proteasome inhibitor used as a positive control. In addition, to further evaluate the anti-proteasome activity of **1-6**, LoVo cells were treated with increasing concentrations of **1** and **4** for 24 h, and then the functioning of each individual proteasome active site, chymotriptic-like (CT-L), trypsin-like (T-L), and caspase-like (C-L) activities were assessed. All copper(II) complexes were barely effective in reducing the CT-L activity of 26S proteasome *in vitro*, eliciting IC_{50} values up to 25 times higher than those calculated for the reference proteasome inhibitor Lactacystin (**Fig. 8 C**). In intact cancer cells, on the contrary, copper complexes proved to be very effective, being able to inhibit 50% of all the three catalytic activities even at low micromolar concentrations. IC_{50} values calculated for CT-L activity were very similar to those of Lactacystin, whereas copper(II) complexes **1** and **4** were significantly more effective than the reference compound in inhibiting T-L and C-L proteasome activities (**Fig. 8 D**).

Copper complexes have been regarded as redox active compounds and redox modulators [50] Actually, copper complexes may catalyze hydrogen peroxide in the form of Fenton-like reactions inside the cell to produce ROS, thus altering cellular redox homeostasis and driving cells towards oxidative stress [51]. On these bases, and tacking into consideration biodistribution studies highlighting the ability of our Cu(II) thiosemicarbazone complexes to accumulate into mitochondria, key organelles involved in cellular redox balance, we also evaluated the ability of **1-6** to alter cellular redox homeostasis. The effects induced by the tested complexes on total cellular sulfhydryl content, total glutathione (GSH + GSSG) and oxidized glutathione (GSSG) levels were assayed in LoVo human colon cancer cells (**Fig. 9 A** and **B**).

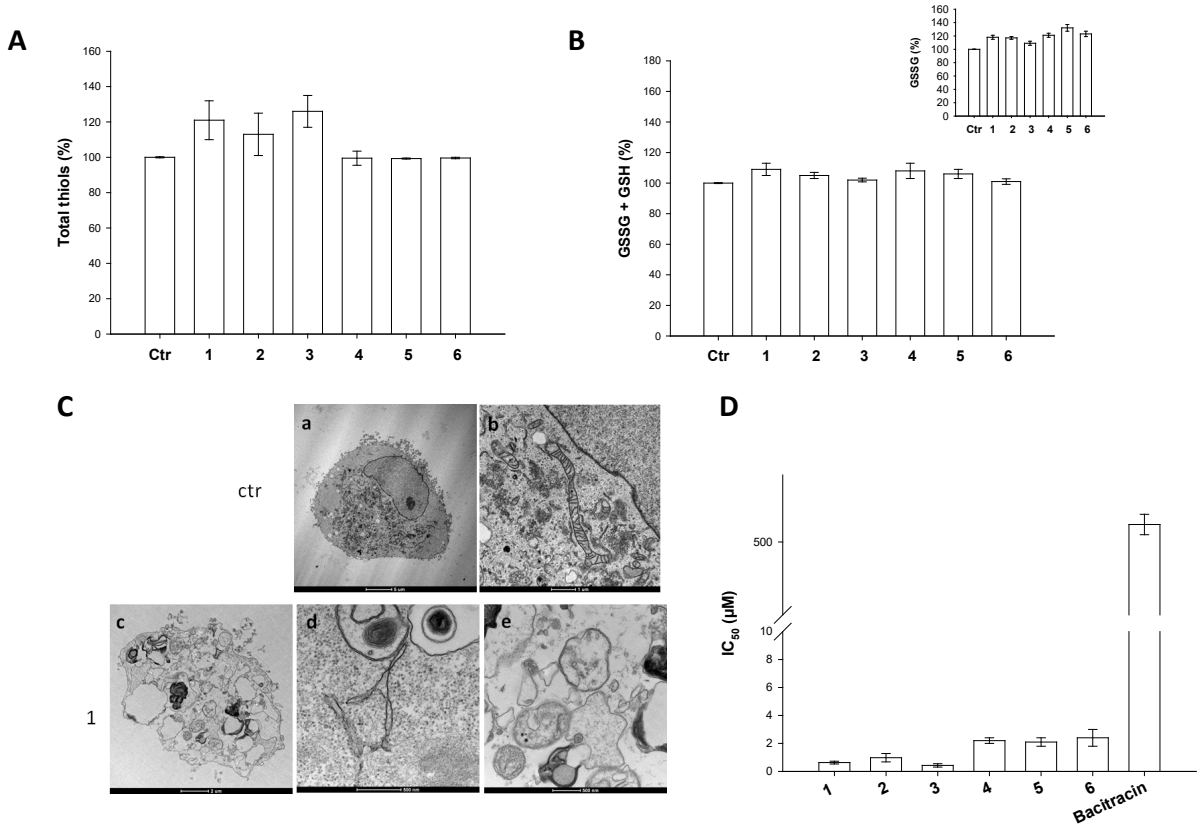

Fig. 9. Mechanistic studies: cellular redox state (A and B), TEM analysis (C) and PDI inhibition (D). (A) Sulfhydryl content in LoVo cancer cells treated for 24 h with IC_{50} concentrations of the tested complexes **1-6**. The sulfhydryl group amount was determined by the DTNB assay. (B) Total and oxidized (insert) glutathione levels in LoVo cancer cells treated with compounds **1-6** at IC_{50} concentrations. Cells were collected and processed as indicated in the Experimental Section. (C) TEM analysis of LoVo cells: a) and b) control cells; c), d) and e) LoVo cells treated for 24 h with IC_{50} concentrations of **1**. (D) PDI inhibition induced by compounds **1-6** was measured by Proteostat PDI assay kit. The PDI inhibitor Bacitracin (0.5 mM) was used as a positive control.

All the tested complexes **1-6** were ineffective in modulating cellular sulfhydryl content and total glutathione content. Interestingly, LoVo cancer cells treated with compounds **1-6** showed higher

levels of oxidized glutathione compared to control cells, and this effect was much more pronounced with complexes **4-6** (**Fig. 9 B**, insert).

In order to characterize the cellular morphological changes induced by the copper(II) thiosemicarbazone compounds, we observed LoVo cancer cells treated for 24 h with IC_{50} concentrations of the most representative compound **1** by using transmission electron microscopy (TEM). Morphological analysis revealed that **1** induced an intense swelling of the mitochondria associated with decreased electron density of the inner membrane and matrix regions (**Fig. 9 C**, panels c, d, and e). In addition, treatment with **1** induced a massive swelling of the ER membrane, which is a clear sign of ER stress.

It is well known that one of the most important protein which acts as an effective crosstalk between ER and mitochondria is Protein Disulfide Isomerase (PDI). PDI has several functions in the ER as catalyst of redox transfer, disulfide isomerization and oxidative protein folding, and as molecular chaperone. Although the impact of binding on the enzymatic activity is not fully characterized, there are reports that PDI is able to bind and reduce copper [52]. Interestingly, PDI expression contributes to copper resistance in various organisms [53]. On these basis, we hypothesized that copper complexes **1-6** interfere with PDI activity, possibly inhibiting its disulfide bond catalytic activity. By monitoring PDI activity in treated LoVo cancer cells, all the **1-6** complexes were found able to potently inhibit the enzyme, being significantly more effective than bacitracin, a well-known inhibitor of PDI activity (**Fig. 9 D**). IC_{50} values calculated for derivatives **1-6** were in the low micromolar range, up to three orders of magnitude lower than those recorded with bacitracin.

In vivo preliminary studies. Owing to the high potential demonstrated by **1-6**, we decided to move a step forward towards preclinical translational studies by performing preliminary *in vivo* anticancer investigations. For these studies, we selected the most promising derivative, the 2-hydroxy-3-methoxybenzaldehyde thiosemicarbazone Cu(II) complex **1**, which showed a very high *in vitro* antitumor activity and a preferential cytotoxicity toward cancer cells. The *in vivo* antitumor activity of **1** was evaluated in a model of solid tumor, the highly aggressive syngeneic murine Lewis Lung

Carcinoma (LLC). Tumor growth inhibition induced by **1** was compared with that promoted by cisplatin. Seven days after tumor inoculation, tumor-bearing mice were randomized into vehicle control and treatment groups. Control mice received the vehicle solution (20% Cremophor EL (v/v), 20% PEG400 (v/v) and 60% saline solution (v/v)) or cisplatin (1.5 mg kg^{-1} in saline solution). The tumor growth was estimated at day 15 and the results are reported in **Table 6**. As an estimation of the adverse side effects, changes in the body weights of tumor-bearing mice were monitored every two days starting from day 7 (**Fig. S23**).

Table 6. *In vivo* antitumor activity. Lewis lung carcinoma (LLC) was implanted i.m. in C57BL mice. After 24 h from tumor implantation, mice were randomly divided into groups of 8 animals (10 controls). Chemotherapy was delayed until the tumor was visible (day 7). Day 15: animals were sacrificed and tumor growth inhibition was determined as the difference in weight of the tumor-bearing leg and the healthy leg (%), referred to control animals. [a]vehicle (20% Cremophor EL (v/v), 20% PEG400 (v/v) and 60% saline solution (v/v))

	Daily dose ($mg \cdot kg^{-1}$)	Average tumor weight (mean±S.D., g)	Inhibition of tumor growth (%)
control[a]	-	0.459±0.13	-
1	3	0.239±0.08	48.0
1	6	0.118±0.09	74.3
CDDP	1.5	0.114±0.08	75.2

Noteworthy, administration of **1** at 3 mg kg^{-1} reduced average tumor growth by half compared to control group whereas at 6 mg kg^{-1} it induced about 75% reduction of the tumor mass, similarly to cisplatin dosed at 1.5 mg kg^{-1}. However, the time course of body weight changes attested that cisplatin induced elevated anorexia (**Figure S13)**. Conversely, treatment with **1** did not induce a substantial body weight loss (<10%) throughout the therapeutic experimentation.

CONCLUSIONS

In the last years, the "old story" of TSCs as anticancer compounds seems to find new perspectives [15]. TSCs and, in particular, their metal complexes could have cellular targets different from cisplatin, opening the expectation to widen the spectrum of action and obtain better selectivity. Until now, TSCs with the 2-pyridil group (**Fig. 1**) have attracted more attention, but here we would like to suggest that also salicylaldehyde derivatives can offer interesting opportunities. In fact, if the activity of $\mathbf{HL^1}$-$\mathbf{HL^6}$ is not significantly different from that of other similar TSCs [54], the activity of the corresponding copper(II) complexes **1**-**6** is remarkable and in some cases in the low nanomolar range. The most effective copper(II) complex **1** was about 466, 1510 and 3480 times more effective than cisplatin against human pancreatic (BxPC3 and PSN1) and colon (HCT-15) cancer cells, and 60 times more active than cisplatin in 3D spheroids of HCT-15 and PSN1 cancer cells. The effect in the resistant spheroid model makes complex **1** a promising drug candidate for further in vivo evaluation, since three-dimensional cell cultures are more similar to real tumors in terms of tissue morphology, biology and gene expression. Worth of note is also that subtle variations in the structure of the ligands can lead to significant differences in activity. In particular, the 3-methoxy 2-hydroxyphenyl thiosemicarbazones form copper(II) complexes (**1**-**3**) on average more active than the 2,3-dihydroxyphenyl derivatives. Speciation studies confirm that the two sets of ligands have different behavior in solution. Moreover, it is suggestive to consider that the important activity of **1**-**3** could be linked to the possibility for these complexes to interact also with the biological relevant sodium ions, as documented in the X-ray structure of $\{Na[CuL^3Cl]_2Cl\}$.

The biochemical data here reported demonstrate that **1-6** are preferentially localized in mitochondria, and that they possess a cellular target that until now has received little attention [55]: Protein Disulfide Isomerase, a copper-binding protein, that is emerging as a new therapeutic target for cancer treatment [56]. The anticancer activity of iron and copper complexes of TSCs has been linked to oxidative stress

induced by ROS production[30,57] or to the inhibition of the enzyme TopoIIα [58]. In a different way, the copper complexes **1-6** do not induce significant oxidative stress, but they are able to potently inhibit PDI (**Fig. 9 D**); remarkably, their IC_{50} values were up to three orders of magnitude lower compared to that of Bacitracin, considered as standard.

Finally, we have to mention the good results obtained in *in vivo* tests. A lot of work has to be done, in particular to improve the solubility of these complexes, but preliminary data are for sure encouraging and clearly indicate that this class of metal-based compounds could be a very promising weapon in the fight against cancer.

EXPERIMENTAL

Materials and methods. Chemistry. Commercial reagents were purchased from Sigma-Aldrich. The purity of the synthesized compounds was determined by elemental analysis and verified to be ≥ 95%. ^{1}H-NMR spectra were recorded at 25 °C on a Bruker Avance 400 FT spectrophotometer. The ATR-IR spectra were recorded by means of a Nicolet-Nexus (Thermo Fisher) spectrophotometer by using a diamond crystal plate in the range of 4000-400 cm^{-1}. Elemental analyses were performed by using a FlashEA 1112 series CHNS/O analyzer (Thermo Fisher) with gas-chromatographic separation. Electrospray mass spectral analyses (ESI-MS) were performed with an electrospray ionization (ESI) time-of-flight Micromass 4LCZ spectrometer. Samples were dissolved in methanol. MS spectra were acquired with a DSQII Thermo Fisher apparatus, equipped with a single quadrupole analyzer in positive EI mode, by means of a DEP-probe (Direct Exposure Probe) equipped with a Re-filament. The UV-vis spectra were collected using a Thermo Evolution 260 Bio spectrophotometer provided with a thermostatting Peltier device, and quartz cuvettes with 1 cm path length.

General synthesis of *HL^1-HL^6*. The thiosemicarbazone ligands were synthesized by condensation of the proper thiosemicarbazide with 2-hydroxy-3-methoxybenzaldehyde or 2,3-dihydroxybenzaldehyde according to procedures already reported for **HL^1** and **HL^4** [59]. Briefly, to

a solution of the aldehyde in absolute ethanol, an equimolar amount of thiosemicarbazide dissolved in the same solvent was added. Few drops of glacial acetic acid were added and the reaction mixture was heated under reflux for 4 h. A precipitate was obtained, which was subsequently filtered, washed with ethanol, and dried under vacuum.

The characterization of **HL[1]** and **HL[4]** is reported in ref. 57.

*2-hydroxy-3-methoxybenzaldehyde-4-phenyl-3-thiosemicarbazone (**HL[2]**).* White powder. Yield = 83%. ^{1}H-NMR (DMSO-d_6, 25°C), δ: 3.82 (s, 3H, OCH_3); 6.79 (t, 1H, ArH); 6.98 (d, 1H, ArH, J_{HH}=7.4); 7.20 (t, 1H, ArH, J_{HH}=7.3); 7.36 (t, 2H, ArH, J_{HH}=7.8); 7.56 (d, 2H, ArH, J_{HH}=7.7); 7.69 (d, 1H, ArH, J_{HH}=7.6); 8.51 (s, 1H, CH=N); 9.26 (s, 1H, OH); 10.03 (s,1H, NH); 11.80 (s, 1H, NH). MS (EI, 70 eV, positive ions) m/z (%) = 301.0 ([M]$^+$, 100). IR (cm^{-1}): ν_{NH} = 3299; $\nu_{C=N}$ = 1594, 1580; $\nu_{C=S}$= 1066, 781. Anal. Calcd. for $C_{15}H_{15}N_3O_2S$: C 59.78, H 5.02, N 13.94, S 10.64. Found: C 59.36, H 4.82, N 13.74, S 11.03.

*2-hydroxy-3-methoxybenzaldehyde-4-ethyl-3-thiosemicarbazone (**HL[3]**).* White powder. Yield = 85%. ^{1}H-NMR (DMSO-d_6, 25°C), δ: 1.13 (t, 3H, $CH_2\underline{CH_3}$); 3.58 (q, 2H, $\underline{CH_2}CH_3$); 3.81 (s, 3H, OCH_3); 6.78 (t, 1H, ArH, J_{HH}=7.9); 6.96 (d, 1H, ArH, J_{HH}=6.6); 7.54 (d, 1H, ArH, J_{HH}=7.3); 8.39 (s, 1H, CH=N); 8.44 (s, br, 1H, NH); 9.20 (s, br, 1H, OH); 11.38 (s, 1H, NH). MS (EI, 70 eV, positive ions) m/z (%) = 253.1 ([M]$^+$, 100). IR (cm^{-1}): ν_{NH} = 3305; $\nu_{C=N}$ = 1522; $\nu_{C=S}$= 1063, 784. Anal. Calcd. for $C_{11}H_{15}N_3O_2S{\cdot}H_2O$: C 48.69, H 6.13, N 15.49, S 11.82. Found: 48.66, H 6.25, N 15.54, S 12.01.

*2,3-dihydroxybenzaldehyde-4-phenyl-3-thiosemicarbazone (**HL[5]**).* White powder. Yield = 83%. ^{1}H-NMR (DMSO-d_6, 25°C), δ: 6.66 (t, 1H, ArH, J_{HH}=6.0); 6.82 (d, 1H, ArH, J_{HH}=6.2); 7.19 (t, 1H, ArH, J_{HH}=6.1); 7.36 (t, 2H, ArH, J_{HH}=6.0); 7.49 (m, 2H, ArH); 7.58 (d, 1H, ArH, J_{HH}=6.3); 8.49 (s, 1H, CH=N); 9.00 (s, 1H, OH); 9.53 (s, 1H, OH); 10.01 (s, 1H, NH); 11.76 (s, 1H, NH). MS (EI, 70 eV, positive ions) m/z (%) = 287.3 ([M]$^+$, 100). IR (cm^{-1}): ν_{OH}+ν_{NH2}= 3442, 3392; ν_{NH} = 3131, 2974; $\nu_{C=N}$ = 1541; $\nu_{C=S}$= 1201, 727. Anal. Calcd. for $C_{14}H_{13}N_3O_2S$: C 58.52, H 4.56, N 14.62, S 11.16. Found: C 58.36, H 4.82, N 14.74, S 11.21.

*2,3-dihydroxybenzaldehyde-4-ethyl-3-thiosemicarbazone (**HL^6**).* White powder. Yield = 92%. ^{1}H-NMR (DMSO-d_6, 25°C), δ: 1.14 (t, 3H, $CH_2\underline{CH_3}$); 3.58 (q, 2H, $\underline{CH_2}CH_3$); 6.66 (t, 1H, ArH, J_{HH}=7.9); 6.81 (d, 1H, ArH, J_{HH}=7.6); 7.36 (d, 1H, ArH, J_{HH}=7.3); 8.37 (s, 1H, CH=N); 8.41 (t, br, 1H, NH); 8.95 (s, br, 1H, OH); 9.52 (s,1H, OH); 11.4 (s, 1H, NH). MS (EI, 70 eV, positive ions) m/z (%) = 239.1 ([M]$^+$, 100). IR (cm^{-1}): ν_{OH}+ν_{NH2}= 3445; ν_{NH} = 3127, 2974; $\nu_{C=N}$ = 1522; $\nu_{C=S}$= 1050, 774. Anal. Calcd. for $C_{10}H_{13}N_3O_2S$: C 50.19, H 5.48, N 17.56, S 13.40. Found: C 50.38, H 5.82, N 17.68, S 13.31.

General synthesis of the complexes *1-6*. 0.15 g of ligand were dissolved in degassed methanol under nitrogen and the pH was adjusted to 8-9 by adding NaOH 1M, resulting in a yellow solution. An equimolar amount of $CuCl_2{\cdot}2H_2O$ in methanol was added and immediately, a dark green precipitate appeared. The suspension was stirred for 4 hours at r.t.. The dark green powder was filtered off and washed with methanol.

(1), [CuL^{1}Cl]·3H_2O. Dark green powder. Yield: 52%. MS-ESI (positive ions) m/z (%) = 287 ([CuL]$^+$, 100); 345 ([CuLCl+Na]$^+$, 70). IR (cm^{-1}): ν_{NH}= 3280, 3168; $\nu_{C=N}$+$\delta_{(N-H)}$ = 1634, 1604; ν_{CS}= 1217. Anal. Calcd. for $C_9H_{10}CuClN_3O_2S{\cdot}3H_2O$: C 28.65; H 4.27; N 11.14. Found: C 28.82; H 4.09; N 10.96. Crystals of [CuL^{1}Cl]·H_2O suitable for X-ray diffraction analysis were obtained by slow evaporation of a methanol solution.

(2), [CuL^{2}Cl]·0.5H_2O. Dark green powder. Yield: 77%. MS-ESI (positive ions) m/z (%) = 363 ([CuL]$^+$, 100); 662 ([CuL_2]$^+$, 10). IR (cm^{-1}): ν_{NH}= 3182, 3019; $\nu_{C=N}$+$\delta_{(N-H)}$= 1605, 1576; ν_{CS}= 1217. Anal. Calcd. for $C_{15}H_{14}CuClN_3O_2S{\cdot}0.5H_2O$: C 44.12; H 3.70; N 10.29. Found: C 44.42; H 3.80; N 10.09.

(3), [CuL^{3}Cl]·1.5 H_2O. Dark green powder. Yield: 71%. MS-ESI (positive ions) m/z (%) = 315 ([CuL]$^+$, 100); 373 ([CuLCl+Na]$^+$, 10). IR (cm^{-1}): ν_{NH} = 3347, 3299; $\nu_{C=N}$+$\delta_{(N-H)}$= 1605, 1586; ν_{CS}= 1219. Anal. Calcd. for $C_{11}H_{14}N_3O_2SCuCl{\cdot}1.5\ H_2O$: C 34.92, H 4.53, N 11.11. Found: C 34.84, H 3.98, N 10.87.

Slow evaporation of mother liqueur leaded to crystals of {Na[CuL^{3}Cl]$_2$Cl} suitable for X-ray diffraction analysis.

(4), [CuL^{4}Cl]·1.5 H_2O. Dark green powder. Yield: 67%. MS-ESI (positive ions) m/z (%) = 273 ([CuL]$^+$, 80); 295 ([CuHLCl+Na]$^+$, 100); 331 ([CuLCl+Na]$^+$, 30). IR (cm^{-1}): ν_{NH} = 3347, 3287; $\nu_{C=N}+\delta_{(N-H)}$= 1640; ν_{CS}= 1230. Anal. Calcd. for $C_8H_8N_3O_2SCu$·1.5 H_2O: C 28.58; H 3.30; N 12.50. Found: C 28.82; H 3.06; N 12.57.

(5), [CuL^{5}Cl]·1.5 H_2O. Dark green powder. Yield: 66%. MS-ESI (positive ions) m/z (%) = 349 ([CuL]$^+$, 100). IR (cm^{-1}): ν_{NH} = 3360, 3207; $\nu_{C=N}+\delta_{(N-H)}$= 1610; ν_{CS}= 1207. Anal. Calcd. for $C_{14}H_{12}N_3O_2SCuCl$· 1.5 H_2O: C 40.78; H 3.67; N 10.19. Found: C 40.85; H 3.53; N 9.97.

(6), [CuL^{6}Cl]·H_2O**.** Dark green powder. Yield: 55%. MS-ESI (positive ions) m/z (%) = 301 ([CuL]$^+$, 100). IR (cm^{-1}): ν_{NH} = 3351, 3271; $\nu_{C=N}+\delta_{(N-H)}$= 1621; ν_{CS}= 1223. Anal. Calcd. for $C_{10}H_{12}N_3O_2SCuCl$· H_2O: C 33.80; H 3.97; N 11.83. Found: C 33.93; H 3.92; N 11.70.

Studies in solution. HEPES 25 mM buffer methanol:water 9:1 (*v/v*) solution at pH 7.4 was prepared as follows: solid HEPES (0.59 g) was suspended in 100 mL of a methanol:water 9:1 (*v/v*) mixture. Few drops of concentrated (10 N) aqueous NaOH solution was added until pH 7.4 was reached, where complete dissolution of the solid was observed. The pH was measured using a Thermo Orion 720A pH-meter connected with a Hamilton glass electrode. A 0.1 M KCl solution in methanol:water 9:1 (*v/v*) was used to fill the reference compartment of the electrode [60]. Calibration of the glass electrode using buffers in methanol:water 9:1 (v/v) solutions was performed immediately before its use [61]. Stock solutions of the ligands **HL^1** and **HL^4** (C_L = *ca*. 1.1 mM) have been prepared by weight in DMF and used within few days. Stock solutions of $CuCl_2$ and $ZnCl_2$ in water (C_{Cu} *ca.* 0.016 M, C_{Zn} *ca.* 0.018 M) were prepared by weight of the salts and their titre determined using standardized EDTA solutions [62]. Titrant metal solutions were obtained by dilution of the stock solutions in methanol:water 9:1 (*v/v*), and prepared at *ca.* 0.55 mM concentration.

UV-visible spectrophotometric titrations. The complex formation equilibria at pH 7.4 for **HL[1]** and **HL[4]** with Cu(II) and Zn(II) were studies by direct spectrophotometric titrations of a solution of the ligands with the metal ions, as follows. Solutions of the ligands (C^0_L = 40 μM) were prepared in the cuvette by diluting the ligands stock solutions in HEPES 25 mM buffer methanol:water 9:1 (*v/v*, pH 7.4). Total volume of samples in the cuvette was *ca*. 2.7 mL. The obtained ligand solutions were titrated with Cu(II) or Zn(II) titrant solutions up to a metal:ligand ratio of 2.4 – 2.7. For each addition of titrant, the absorption spectrum was collected in the 250-500 nm range. The equilibria of the Cu(II)/Zn(II)/**HL[1]** system were studied by a competitive UV-Visible spectrophotometric titration, as follows. A solution of the ligand **HL[1]** (C^0_L = 41 μM) was prepared in the cuvette by diluting the ligand stock solution in HEPES 25 mM buffer methanol:water 9:1 (*v/v*, pH 7.4). A proper amount of the Zn(II) stock solution was added to the ligand solution to obtain a Zn(II) and **HL[1]** in 2:1 ratio. The obtained titrant solution was titrated with Cu(II) up to a Cu(II):ligand ratio of 1.1. In all experiments, for each addition of the titrant the absorption spectrum was collected in the 250-500 nm range. All titrations were performed in triplicate.

Job's plot experiments were carried out by preparing 11 solutions with constant $C_{Cu/Zn} + C_L$ (*ca*. 40 μM, L = **HL[1]** or **HL[4]**), and variable $\chi = C_L/(C_L+C_{Cu/Zn})$ molar fractions in the 0 – 1 range. All samples were prepared in HEPES 25 mM buffer methanol:water 9:1 (*v/v*) solution at pH 7.4.

The logarithms of the conditional stability constants were calculated from the spectral dataset using the HypSpec2014 software [63,64]. For each system, data from different titrations were treated together. In the treatment of the competitive titration of the Zn(II):**HL[1]** system with Cu(II), the formation constants and the molar absorption spectra of the [Zn(L4)] and [Zn(L4)$_2$] complexes (charges omitted, see below) were used as fixed parameters. In all other titrations the molar spectrum of the ligand has been used as the only fixed parameter. Speciation diagrams were calculated using the Hyss 2009 software [65].

Crystallography. Single crystals of [CuL[1]Cl]·H$_2$O and {Na[CuL[3]Cl]$_2$Cl} were mounted on a glass fibre and the intensity data were collected with a SMART APEX2 diffractometer equipped with a

Bruker AXS CCD detector using Mo-Ka radiation and a graphite crystal monochromator [λ(Mo-Kα) = 0.71073 Å]. The SAINT [66] software was used for the integration of reflection intensities and scaling, and SADABS [67] for the absorption correction. The structures were solved by direct methods using SIR97 [68] and refined by full-matrix least-squares on all F2 using SHELXL97 [69] implemented in the WinGX package [70]. All the non-hydrogen atoms in the molecules were refined anisotropically. The hydrogen atoms were partly found and partly placed in ideal positions using riding models. The structures were solved by direct methods and difference Fourier synthesis using the SHELX suite of programs as implemented within the WINGX software. Thermal ellipsoid plots were generated using the program ORTEP-333 integrated within the WinGX suite of programs. CCDC1816442-1816443 contain the supplementary crystallographic data of $[CuL^1Cl]\cdot H_2O$ and $\{Na[CuL^3Cl]_2Cl\}$ (http://www.ccdc.cam.ac.uk/data_request/cif).

Experiments with Human Cells. Complexes and organic ligands were solubilized in stock DMSO solutions (10 mg/mL) and added to the culture medium to a final solvent concentration of 0.5%, which had no effects on cell viability. Cisplatin (CDDP) and oxaliplatin were solubilized in 0.9% NaCl solutions. MTT (3-(4,5-dimethylthiazol-2-yl)-2,5-diphenyltetrazolium bromide), fluorogenic peptide proteasomal substrates (N-Suc-Leu-Leu-Val-Tyr-AMC, Boc-Gln-Ala-Arg-AMC, and Z-Leu-Leu-Glu-AMC; AMC = 7-amido-4-methylcoumarin), cisplatin and oxaliplatin were obtained from Sigma Chemical Co, St. Louis, USA.

Cell Cultures. Human colon (HCT-15 and LoVo) carcinoma cell lines along with human melanoma (A375) and nontransformed embryonic kidney (HEK293) cells were obtained from American Type Culture Collection (ATCC, Rockville, MD, USA). Human pancreatic (BxPC3 and PSN1) carcinoma cells were obtained from European Collection of Cell Culture (ECACC, Salisbury, UK). The human thyroid carcinoma cell line (BCPAP) was provided by the Leibniz-Institut DSMZ-Deutsche Sammlung von Mikroorganismen und Zellkulturen GmbH (Braunschweig, Germany). Human ovarian 2008 cancer cells were kindly provided by Prof. G. Marverti (Dept. of Biomedical Science of Modena University, Modena, Italy). The LoVo-OXP cells were obtained as previously described

[71]. Cell lines were maintained in culture in the logarithmic phase at 37 °C in a 5% carbon dioxide atmosphere using the following media added of 10% fetal calf serum (Euroclone, Milan, Italy), antibiotics (50 units/mL penicillin and 50 μg/mL streptomycin), and 2 mM L-glutamine: (i) RPMI-1640 medium (Euroclone) for HCT-15, PSN1, BCPAP, BxPC3 and 2008 cells; (ii) F-12 HAM'S (Sigma Chemical Co.) for LoVo and LoVo-OXP cells; iii) DMEM (Sigma Chemical Co.) for A375 and HEK293 cells.

Spheroid Cultures. Spheroid cultures were obtained by seeding 2.5×10^3 HCT-15 or PSN1 cells/well in round bottom non-tissue culture treated 96 well-plate (Greiner Bio-one, Kremsmünster, Austria) in phenol red free RPMI-1640 medium (Sigma Chemical Co.), containing 10% FCS and supplemented with 20% methyl cellulose stock solution.

MTT Assay. The growth inhibitory effect towards 2D tumor cell lines was evaluated by means of the MTT assay as previously described [72]. IC50 values were calculated by four parameter logistic (4-PL) model.

Acid Phosphatase (APH) Assay. An APH modified assay was used for determining cell viability in 3D spheroids, as previously described [73]. IC50 values were calculated with 4-PL model.

Cellular accumulation and distribution. LoVo cells (2.5×106) were seeded in 75 cm^2 flasks in growth medium (20 mL). After overnight incubation, the medium was replaced and the cells were treated with the tested compounds for 24 or 36 h. Cell monolayers were washed with cold PBS, harvested and counted. Cell nuclei were isolated by means of nuclei isolation kit Nuclei EZ Prep (Sigma Co.) and also cellular mitochondrial fractions were isolated by Mitochondria Isolation Kit (Sigma Co.). The samples were treated with highly pure nitric acid (Cu: ≤0.005 $\mu g \cdot kg^{-1}$, TraceSELECT® Ultra, Sigma Chemical Co.) and transferred into a microwave teflon vessel. Afterwards, samples were mineralized by using a speed wave MWS-3 Berghof instrument (Eningen, Germany). After cooling, each mineralized sample was analyzed for copper content by means of a Varian AA Duo graphite furnace atomic absorption spectrometer (Varian, Palo Alto, CA; USA), at

324 nm. The calibration curve was obtained using known concentrations of standard solutions purchased from Sigma Chemical Co.

Comet Assay. Single-cell gel electrophoresis for detection of DNA damage was performed using the Comet assay reagent kit (Trevigen Inc., Gaithersburg, MD, US) according to the manufacturer's instructions. Briefly, LoVo (10^5) cells were seeded in 25 cm^2 flasks in growth medium (6 mL). After 24 h, cells were incubated for 6 h with IC_{50} concentrations of tested compounds. Subsequently, cells were washed twice with cold PBS, harvested, centrifuged, and resuspended at 1×10^5 cell/mL in 1% low melting point agarose (LMPA, Trevigen). Then 50 μL of cells−LMPA mixture were layered onto frozen microscope slides, which were pre-coated with 1% normal agarose. After the agar had been allowed to set at 4 °C, the slides were immersed in lysis buffer (100 mM Na_2EDTA, 2.5 M NaCl, 10 mM Tris pH 10.0, and 1% Triton X-100) for 1 h at 4 °C. The slides were then incubated in an alkaline electrophoresis solution (1 mM EDTA, 300 mM NaOH, pH > 13) at 4 °C for 40 min, followed by electrophoresis (1 V/cm) at 4 °C for 30 min. The slides were washed with a neutralization buffer three times before immersion in absolute ethanol for 20 min and air-dried at room temperature. The DNA was stained with SYBR Green (1 μg/mL) for 5 min at 4 °C. A total of 25 comets per slide, randomly captured, were examined at 40x magnification in a fluorescence microscope (Olympus BX41, Milano, Italy; excitation, 495 nm; emission, 521 nm) connected through a black and white camera to a computer-based image analysis system. DNA damage was measured as tail length (distance of DNA migration from the middle of the body of the nuclear core) using Cell-F software (Olympus).

Proteasome activity

In vitro inhibition of purified 26S proteasome. The purified rabbit 26S proteasome (Sigma Aldrich) was incubated for 60 min at 37 °C in an assay buffer (50 mM Tris-HCl, pH 7.5, 250 mM sucrose, 5 mM $MgCl_2$, 1 mM DTT, and 0.5 mM EDTA), in the presence of increasing concentrations of the tested complexes or Lactacystin. Afterwards, fluorogenic peptides were added and substrate hydrolysis was measured after 30 min by monitoring spectrofluorometrically the release of AMC (excitation at 370 nm, emission at 460 nm).

Inhibition of 26S proteasome in intact cancer cells. Human colon adenocarcinoma LoVo (10^6) cells were treated for 24 h with IC_{50} concentrations of tested compounds. Afterward, cells were harvested and homogenized in a lysis buffer (50 mM Tris-HCl, pH 7.5, 250 mM sucrose, 5 mM $MgCl_2$, 1 mM DTT, and 0.5 mM EDTA), and the protein concentration in the cytosolic extract was determined by the BioRad protein assay (BioRad). Protein aliquots (100 μg) were stained at 37 °C for 30 min with a fluorescent proteasome substrate specific for CT-like activity and the hydrolysis was measured as described above.

Quantification of thiols. LoVo cells (2×10^5) were seeded in a six-well plate in growth medium (4 mL). After 24 h, cells were incubated for 24 h with IC_{50} concentrations of tested compounds. Subsequently, the thiol content was measured as previously described [74].

Total and oxidized intracellular glutathione. LoVo cells (3.5×10^5) were seeded in 6-well microplates in growth medium (4 mL). Following 24 h of exposure with IC_{50} concentrations of tested complexes, cells were washed twice with PBS, treated with 6% metaphosphoric acid and scraped. Samples were centrifuged and the supernatants were neutralized with Na_3PO_4 and assayed for total and oxidized glutathione following the procedure reported by Bindoli et al [75]. Aliquots of pellets were dissolved in RIPA buffer and the protein content was determined.

Protein disulfide isomerase (PDI) activity. The reductase activity of PDI was assayed by measuring the PDI-catalysed reduction of insulin in the presence of increasing concentrations of the tested compounds by using PROTEOSTAT PDI assay kit (Enzo Life Sciences, Lausen, Switzerland). Experiments were performed according to the manufacturer's instructions. Briefly, copper complexes or Bacitracin (at increasing concentrations) were added to an insulin PDI solution. Subsequently, DTT was added to start PDI reduction activity and after 30 min of incubation, the reaction was stopped by adding the stop reagent mixture. The insulin precipitate was labelled with the fluorescent Proteostat PDI detection reagent and fluorescence intensity was measured at 500 nm excitation and 603 nm emission. IC_{50} values were calculated by 4-PL model.

Transmission electron microscopy (TEM) analyses. About 10^6 LoVo cells were seeded in 24-well plates and, after 24 h incubation, were treated with IC_{50} concentrations of tested compounds and incubated for additional 24 h. Cells were then washed with cold PBS, harvested and directly fixed with 1.5% glutaraldehyde buffer with 0.2 M sodium cacodylate, pH 7.4. After washing with buffer and postfixation with 1% OsO_4 in 0.2 M cacodylate buffer, specimens were dehydrated and embedded in epoxy resin (Epon Araldite). Sagittal serial sections (1 μm) were counterstained with toluidine blue; thin sections (90 nm) were given contrast by staining with uranyl acetate and lead citrate. Micrographs were taken with a Hitachi H-600 electron microscope (Hitachi, Tokyo, Japan) operating at 75 kV. All photos were typeset in Corel Draw 11.

Nuclear DNA Fragmentation. LoVo cells (10^4/well) were treated in a 96-well plate at 37 °C for 24 h with IC_{50} doses of tested compounds. Afterward, the plate was centrifuged for 10 min, the supernatant removed, and the pellet treated according to the manufacturer's instructions of an ELISAplus cell death detection kit (Roche). The extent of nuclear fragmentation was measured in a plate reader following absorbance at 405 minus 492 nm.

Experiments with animals. All experiments were reviewed and approved by the internal Review Board (OPBA) and authorized by the Italian Ministry of Health (authorization n. 640/2016-PR), accordingly with the current national and European regulations and guidelines for the care and use of laboratory animals (D.L. 26/2014; 86/609/EEC Directive).

***In vivo* anticancer activity toward Lewis Lung Carcinoma (LLC).** The mice were purchased from Charles River, Italy, housed in steel cages under controlled environmental conditions (constant temperature, humidity, and 12 h dark/light cycle), and alimented with commercial standard feed and tap water ad libitum. The LLC cell line was purchased from ECACC, United Kingdom. The LLC cell line was maintained in DMEM (Euroclone, Pero, Italy) supplemented with 10% heat-inactivated foetal bovine serum (Euroclone, Pero, Italy), 10 mM L-glutamine, 100 U/mL penicillin, and 100 μg/mL streptomycin in a 5% CO_2 air incubator at 37 °C. The LLC was implanted intramuscularly

(i.m.) as a 2×10^6 cell inoculum into the right hind leg of 8-week old male and female C57BL mice (24 ± 3 g body weight). After 7 days from tumor implantation (tumor visible), mice were randomly divided into 4 groups (8 animals per group) and treated with a daily i.p. injection of **1** (3 and 6 mg kg^{-1} in 20% Cremophor EL (v/v), 30% PEG400 (v/v) and 50% saline solution (v/v)), cisplatin (1.5 mg kg^{-1} in 0.9% NaCl solution), or the vehicle solution 20% Cremophor EL (v/v), 30% PEG400 (v/v) and 50% saline solution (v/v). At day 15, animals were sacrificed, the legs were amputated at the proximal end of the femur, and the inhibition of tumor growth was determined according to the difference in weight of the tumor-bearing leg and the healthy leg of the animals expressed as a percentage referring to the control animals. Body weight measured every 2 days, starting from day 7, was taken as a parameter for systemic toxicity. All of the values are the means ± SD of not less than three measurements. Multiple comparisons were made by the Tukey−Kramer test (**, $p < 0.01$; * $p < 0.05$).

ASSOCIATED CONTENT

Supporting Information. Supplementary data to this article can be found online at https://doi.org/XXX. ESI-MS of complexes **1-6**, UV-visible spectra, Job's plots, body weights changes graph (PDF), bond distances and angles for crystal structures.

■ AUTHOR INFORMATION

Corresponding Authors:

*valentina.gandin@unipd.it

*dominga.rogolino@unipr.it

These authors contributed equally to the work

ORCID

Valentina Gandin: 0000-0003-0442-0670

Dominga Rogolino: 0000-0003-2295-5783

Author Contributions

The manuscript was written through contributions of all authors. All authors have given approval to the final version of the manuscript.

Notes

The authors declare no competing financial interest.

ACKNOWLEDGMENTS

The authors thank “Centro Interfacoltà Misure Giuseppe Casnati” of the University of Parma for facilities. This work has benefited from the equipment and framework of the COMP-HUB Initiative, funded by the ‘Departments of Excellence’ program of the Italian Ministry for Education, University and Research (MIUR, 2018-2022).

REFERENCES

[1] Lippard, S. J. The inorganic side of chemical biology. *Nat. Chem. Biol.* **2006**, *2*, 504-507. DOI: 10.1038/nchembio1006-504

[2] Barry, N.P. E.; Sadler, P. J. Exploration of the medical periodic table: towards new targets. *Chem. Commun.* **2013**, *49*, 5106-5131. DOI: 10.1039/C3CC41143E

[3] Wang, D.; Lippard, S. J. Cellular processing of platinum anticancer drugs. *Nat. Rev. Drug Discov.* **2005**, *4*, 307-320. DOI: 10.1038/nrd1691

[4] Ho, J. W. Potential and cytotoxicity of cis-platinum complex with anti-tumor activity in combination therapy. *Recent Pat Anticancer Drug Discov.* **2006**, *1*, 129-134.

[5] Brabec, V.; Kasparkova, J. Modifications of DNA by platinum complexes. *Drug Resistance Updates* **2005**, *8*, 131-146. DOI: 10.1016/j.drup.2005.04.006

[6] Han Ang, W.; Khalaila, I.; Allardyce, C.S.; Juillerat-Jeanneret, L.; Dyson, P.J. *J. Am. Chem. Soc.* **2005**, 127, 1382-1383. DOI: 10.1021/ja0432618

[7] Frezza, M.; Hindo, S.; Chen, D.; Davenport, A.; Schmitt, S.; Tomco, D.; Dou, Q. P. Novel metals and metal complexes as platforms for cancer therapy. *Curr. Pharm. Des.* **2010**, 16, 1813-1825. DOI: 10.2174/138161210791209009

[8] Diez, M.; Arroyo, M.; Cerdan, F. J.; Munoz, M.; Martin, M. A.; Balibrea, J. L. Serum and Tissue Trace Metal Levels in Lung Cancer. *Oncology* **1989**, *46*, 230-234. DOI: 10.1159/000226722

[9] Geraki, K.; Farquharson, M. J.; Bradley, D. A. Concentrations of Fe, Cu and Zn in breast tissue: a synchrotron XRF study. *Phys. Med. Biol.* **2002**, *47*, 2327. DOI: 10.1088/0031-9155/47/13/310

[10] Yoshida, D.; Ikeda, Y.; Nakazawa, S. Quantitative analysis of copper, zinc and copper/zinc ratio in selected human brain tumors. *J. Neuro-Oncol.* **1993**, *16*, 109-115. DOI: 10.1007/BF01324697

[11] Xie, H.; Kang, Y. J. Role of copper in angiogenesis and its medicinal implications. *Curr. Med. Chem.* **2009**, *16*, 1304-1314. DOI: 10.2174/092986709787846622

[12] Santini, C.; Pellei, M.; Gandin, V.; Porchia, M.; Tisato, F.; Marzano, C. Advances in copper complexes as anticancer agents. *Chem. Rev.* **2014**, 114, 815-862. DOI: 10.1021/cr400135x

[13] Marzano, C.; Pellei, M.; Tisato, F.; Santini, C. Copper complexes as anticancer agents. *Anticancer Agents Med. Chem*. **2009**, *9*, 185-211. DOI: 10.2174/187152009787313837

[14] Tardito, S.; Marchiò, L. Copper compounds in anticancer strategies. *Curr. Med. Chem.* **2009**, *16*, 1325-48. DOI: 10.2174/092986709787846532

[15] Yu, Y.; Kalinowski, D.S.; Kovacevic, Z.; Siafakas, R.A.; Jansson, P.J.; Stefani, C.; Lovejoy, D.B.; Sharpe, P.S.; Bernhardt, P.V.; Richardson, D.R. Thiosemicarbazones from the old to new: iron chelators that are more than just ribonucleotide reductase inhibitors. *J. Med. Chem.* **2009**, *52*, 5271-5294. DOI: 10.1021/jm900552r

[16] Pelosi, G. Thiosemicarbazone metal complexes: from structure to activity. *Open Crystallogr. J.* **2010**, *3*, 16-28. DOI: 10.2174/1874846501003010016

[17] Kalinowski, D. S.; Quach, P.; Richardson, D. R. Thiosemicarbazones: the new wave in cancer treatment. *Future Med. Chem.* **2009**, *1*, 1143-1151. DOI: 10.4155/fmc.09.80

[18] Kunos, C. A.; Chu, E.; Beumer, J. H.; Sznol, M.; Ivy, S. P. Phase I trial of daily triapine in combination with cisplatin chemotherapy for advanced-stage malignancies. *Cancer Chemother. Pharmacol.* **2017**, *79*, 201-207. DOI: 10.1007/s00280-016-3200-x

[19] Zeidner, J. F.; Karp, J. E.; Blackford, A. L.; Smith, B. D.; Gojo, I.; Gore, S. D.; Levis, M. J.; Carraway, H. E.; Greer, J. M.; Ivy, S. P.; Pratz K. W.; McDevitt, M. A. A phase II trial of sequential ribonucleotide reductase inhibition in aggressive myeloproliferative neoplasms. *Haematologica,* **2014**, *99*, 672-678. DOI: 10.3324/haematol.2013.097246

[20] Jansson, P. J.; Kalinowski, D. S.; Lane, D. J. R.; Kovacevic, Z.; Seebacher, N. A.; Fouani, L.; Sahni, S.; Merlot, A. M.; Richardson, D. R. The renaissance of polypharmacology in the development of anti-cancer therapeutics: Inhibition of the "Triad of Death" in cancer by Di-2-pyridylketone thiosemicarbazones. *Pharmacol. Res.* **2015**, *100*, 255-260. DOI: 10.1016/j.phrs.2015.08.013

[21] Salim, K. Y.; Danter, W. R.; Maleki, V. S.; Koropatnick, J. COTI-2, a novel small molecule that is active against multiple human cancer cell lines *in vitro* and *in vivo*. *Oncotarget* **2016**, *7*, 41363-41379. DOI: 10.18632/oncotarget.9133.

[22] Rao, V.A.; Klein, S.R.; Agama, K.K.; Toyoda, E.; Adachi, N.; Pommier, Y.; Shacter, E.B. The iron chelator Dp44mT causes DNA damage and selective inhibition of topoisomerase II alpha in breast cancer cells. *Cancer Res.* **2009**, *69*, 948-957. DOI: 10.1158/0008-5472.CAN-08-1437

[23] Malarz, K.; Mrozek-Wilczkiewicz, A.; Serda, M.; Rejmund, M.; Polanski, J.; Musiol, R. The role of oxidative stress in activity of anticancer thiosemicarbazones, *Oncotarget* **2018**, *9*, 477-486. DOI: 10.18632/oncotarget.24844

[24] Mrozek-Wilczkiewicz, A.; Malarz, K.; Rejmund, M.; Polanski, J.; Musiol R. Anticancer activity of the thiosemicarbazones that are based on di-2-pyridine ketone and quinoline moiety. *Eur. J. Med. Chem.* **2019**, *171*, 180-194. DOI: 10.1016/j.ejmech.2019.03.027

[25] Garcia-Tojal, J.; Gil-Garcia, R.; Gomez-Saiz, P.; Ugalde, M. Pyridine-2-carbaldehyde thiosemicarbazone copper system: extending some findings to other thiosemicarbazone and coordination compounds. *Curr. Inorg. Chem.* **2011**, *1*, 189-210. DOI: 10.2174/1877944111101020189

[26] Enyedy, É. A.; Zsigó, É.; Nagy, N. V.; Kowol, C. R.; Roller, A.; Keppler, B. K.; Kiss, T. Complex-formation ability of salicylaldehyde thiosemicarbazone towards ZnII, CuII, FeII, FeIII and GaIII Ions. *Eur. J. Inorg. Chem.* **2012**, 4036-4047. DOI: 10.1002/ejic.201200360

[27] Beraldo, H.; Gambino, D. The wide pharmacological versatility of semicarbazones, thiosemicarbazones and their metal complexes. *Mini-Rev. Med. Chem.* **2004**, *4*, 31-39. DOI: 10.2174/1389557043487484

[28] Popovic-Bijelic, A.; Kowol, C. R.; Lind, M. E. S.; Luo, J.; Himo, F.; Enyedy, E. A.; Arion, V.B.; Graeslund, A. Ribonucleotide reductase inhibition by metal complexes of Triapine (3-aminopyridine-2-carboxaldehyde thiosemicarbazone): a combined experimental and theoretical study. *J. Inorg. Biochem.* **2011**, *105*, 1422-1431. DOI: 10.1016/j.jinorgbio.2011.07.003

[29] Yu, Y.; Rahmanto, Y. S.; Hawkins, C. L.; Richardson, D. R. The potent and novel thiosemicarbazone chelators di-2-pyridylketone-4,4-dimethyl-3-thiosemicarbazone and 2-benzoylpyridine-4,4-dimethyl-3-thiosemicarbazone affect crucial thiol systems required for ribonucleotide reductase activity. *Mol. Pharmacol.* **2011**, *79*, 921-931. DOI: 10.1124/mol.111.071324

[30] Jansson, P. J.; Sharpe, P. C.; Bernhardt, P. V.; Richardson, D. R. Novel thiosemicarbazones of the ApT and DpT series and their copper complexes: identification of pronounced redox activity and characterization of their antitumor activity. *J. Med. Chem.* **2010**, *53*, 5759-5769. DOI: 10.1021/jm100561b

[31] Bernhardt, P. V.; Sharpe, P. C.; Islam, M.; Lovejoy, D. B.; Kalinowski, D. S.; Richardson, D. R. Iron chelators of the dipyridylketone thiosemicarbazone class: precomplexation and transmetallation effects on anticancer activity. *J. Med. Chem.* **2009**, *52*, 407-415. DOI: 10.1021/jm801012z

[32] Denoyer, D.; Masaldan, S.; La Fontaine, S.; Cater, M.A. Targeting copper in cancer therapy: 'Copper that Cancer'. *Metallomics*, **2015**, *7*, 1459-1476. DOI:10.1039/C5MT00149H

[33] Akladios, F.N.; Andrew, S.D.; Parkinson, C. J. Increased generation of intracellular reactive oxygen species initiates selective cytotoxicity against the MCF-7 cell line resultant from redox active combination therapy using copper-thiosemicarbazone complexes, *J. Biol. Inorg. Chem.* **2016**, *21*, 407-419. DOI: 10.1007/s00775-016-1350-2

[34] Kowol, C. R.; Heffeter, P.; Miklos, W.; Gille, L.; Trondl, R.; Cappellacci, L.; Berger, W.; Keppler, B.K. Mechanisms underlying reductant-induced reactive oxygen species formation by anticancer copper(II) compounds, *J. Biol. Inorg. Chem.*, **2012**, *17,* 409-423. DOI: 10.1007/s00775-011-0864-x

[35] Wang, J.; Luo, C.; Shan, C.; You, Q.; Lu, J.J.; Elf, S.; Zhou, Y.; Wen, Y.; Vinkenborg, J.L.; Fan, J.; Kang, H.; Lin, R.; Han, D.; Xie, Y.; Karpus, J.; Chen, S.; Ouyang, S.; Luan, C.; Zhang, N.; Ding, H.; Merkx, M.; Liu, H.; Chen, J.; Jiang, H.; He, C. Inhibition of human copper trafficking by a small molecule significantly attenuates cancer cell proliferation. *Nat. Chem.*, **2015**, *7*, 968-979.

[36] Dilovic´, I.; Rubcˇic´, M.; Vrdoljak, V.; Pavelic´, S. K.; Kralj M., Piantanidab, I.; Cindric´, M. Novel thiosemicarbazone derivatives as potential antitumor agents: Synthesis, physicochemical and structural properties, DNA interactions and antiproliferative activity. *Bioorg. Med. Chem.* **2008**, *16*, 5189-5198. DOI: 10.1016/j.bmc.2008.03.006

[37] Qi, J.; Gou, Y.; Zhang, Y.; Yang, K.; Chen, S.; Liu, L.; Wu, X.; Wang, T.; Zhang, W.; Yang, F. Developing Anticancer Ferric Prodrugs Based on the N-Donor Residues of Human Serum Albumin Carrier IIA Subdomain. *J. Med. Chem.* **2016**, *59*, 7497-7511. DOI: 10.1021/acs.jmedchem.6b00509

[38] Gatti, A.; Habtemariam, A.; Romero-Canelón, I.; Song, J.-I.; Heer, B.; Clarkson, G. J.; Rogolino, D.; Sadler, P. J.; Carcelli, M. Half-Sandwich Arene Ruthenium(II) and Osmium(II) Thiosemicarbazone Complexes: Solution Behavior and Antiproliferative Activity. *Organomet.*, **2018**, *37*, 891-899. DOI: 10.1021/acs.organomet.7b00875

[39] Zhang, Z.; Gou, Y.; Wang, J.; Yang, K.; Qi, J.; Zhou, Z.; Liang, S.; Liang, H.; Yang, F. Four copper(II) compounds synthesized by anion regulation: structure, anticancer function and anticancer mechanism. *European Journal of Medicinal Chemistry*, **2016**, *121,* 399-409. DOI: 10.1016/j.ejmech.2016.05.021

[40] Belicchi-Ferrari, M.; Bisceglie, F.; Buschini, A.; Franzoni, S.; Pelosi, G.; Pinelli, S.; Tarasconi, P.; Tavone, M. Synthesis, structural characterization and antiproliferative and toxic bio-activities of copper(II) and nickel(II) citronellal N4-ethylmorpholine thiosemicarbazonates. *J. Inorg. Biochem.* **2010**, *104,* 199-206. DOI: 10.1016/j.jinorgbio.2009.11.002

[41] Dobrova, A.; Platzer, S.; Bacher, F.; Milunovic, M. N. M.; Dobrov, A.; Spengler, G.; Enyedy, É. A.; Novitchid, G.; Arion, V. B. Structure–antiproliferative activity studies on L-proline- and homoproline-4-N-pyrrolidine-3- thiosemicarbazone hybrids and their nickel(II), palladium(II) and copper(II) complexes. *Dalton Trans.*, **2016**, *45*, 13427-13439. DOI: 10.1039/C6DT02784A

[42] Rogolino, D.; Gatti, A.; Carcelli, M.; Pelosi, G.; Bisceglie, F.; Restivo, F. M.; Degola, F.; Buschini, A.; Montalbano, S.; Feretti, D.; Zani, C. Thiosemicarbazone scaffold for the design of

antifungal and antiaflatoxigenic agents: evaluation of ligands and related copper complex. *Sci. Rep. 2017*, *7*, 11214. DOI:10.1038/s41598-017-11716-w

[43] Sen, S.; Shit, S., Mitra; S.; Batten, S. R. Structural and spectral studies of a new copper(II) complex with a tridentate thiosemicarbazone ligand. *Struct. Chem.* **2008**, 19, 137–142. doi:10.1007/s11224-007-9263-x

[44] Sokołowska, M.; Bal, W. Cu(II) complexation by "non-coordinating" N-2-hydroxyethylpiperazine-N'-2-ethanesulfonic acid (HEPES buffer). *J. Inorg. Biochem.* **2005**, 1653-1660. DOI: 10.1016/j.jinorgbio.2005.05.007.

[45] Anwar, Z. M. Complexation Equilibria of Zn(II), Pb(II) and Cd(II) with Reduced Glutathione (GSH) and Biologically Important Zwitterionic Buffers. *J. Chinese Chem. Soc.* **2005**, *52*, 863-871 DOI: 10.1002/jccs.200500121.

[46] Ferreira, C. M. H.; Pinto, I. S. S.; Soares, E. V.; Soares, H. M. V. M. (Un)suitability of the use of pH buffers in biological, biochemical and environmental studies and their interaction with metal ions – a review. *RSC Adv.* **2015**, *5*, 30989-31003. DOI: 10.1039/C4RA15453C.

[47] Raymond, E.; Faivre, S.; Chaney, S.; Woynarowski, J.; Cvitkovic, E. Cellular and Molecular Pharmacology of Oxaliplatin. *Mol. Cancer Ther.* **2002**, *1*, 227-235.

[48] Kankotia, S.; Stacpoole, P. W. Dichloroacetate and cancer: new home for an orphan drug? *Biochim. Biophys. Acta*, **2014**, *1846*, 617-629. DOI: 10.1016/j.bbcan.2014.08.005

49 Adsule, S.; Barve, V.; Chen, D.; Ahmed; F., Dou Q.P.; Padhye S.; Sarkar, F.H. Novel Schiff Base Copper Complexes of Quinoline-2 Carboxaldehyde as Proteasome Inhibitors in Human Prostate Cancer Cells. *J. Med. Chem.* **2006**, 49, 7242-7246. DOI: 10.1021/jm0607121

[50] Allensworth, J.L.; Evans, M.K.; Bertucci, F.; Aldrich, A.J.; Festa, R.A.; Finetti, P.; Ueno, N.T.; Safi, R.; McDonnell, D.P.; Thiele, D.J.; Van Laere, S.; Devi, G.R. Disulfiram (DSF) acts as a copper ionophore to induce copper-dependent oxidative stress and mediate anti-tumor efficacy in inflammatory breast cancer. *Mol Oncol.* **2015**, *9*, 1155-1168. DOI: 10.1016/j.molonc.2015.02.007

[51] Öhrvik, H.; Aaseth, J.; Horn, N. Orchestration of dynamic copper navigation – new and missing pieces. *Metallomics* **2017**, *9*, 1204-1229. DOI: 10.1039/c7mt00010c

[52] Narindrasorasak, S.; Yao, P.; Sarkar, B. Protein disulfide isomerase, a multifunctional protein chaperone, shows copper-binding activity. *Biochem. Biophys. Res. Commun.* **2003**, *311*, 405-414. DOI: 10.1016/j.bbrc.2003.09.226

[53] Furlong, E.J.; Lo, A.W. ; Kurth, F.; Premkumar, L.; Totsika, M.; Achard, M.E.S.; Halili, M.A.; Heras, B.; Whitten, A.E.; Choudhury, H.G.; Schembri, M.A.; Martin, J.L. A shape-shifting redox foldase contributes to *Proteus mirabilis* copper resistance. *Nat Commun.* **2017**, 8, 16065. DOI: 10.1038/ncomms16065

[54] Hu, B.; Wang, B.; Zhao, B.; Guo, Q.; Li, Z.-H.; Zhang, X.-H.; Liu, G.-Y.; Liu, Y.; Tang, Y.; Luo, F.; Du, Y.; Chen, Y.-X.; Ma, L.-Y.; Liu, H.-M. Thiosemicarbazone-based selective proliferation inactivators inhibit gastric cancer cell growth, invasion, and migration. *Med. Chem. Comm.* **2017**, *8*, 2173-2180. DOI: 10.1039/c7md00353f

[55] Hager, S.; Korbula, K.; Bielec, B.; Grusch, M.; Pirker, C.; Schosserer, M.; Liendl, L.; Lang, M.; Grillari, J.; Nowikovsky, K.; Pape, V. F. S.; Mohr, T.; Szakács, G.; Keppler, B. K.; Berger, W.; Kowol, C. R.; Heffeter, P. The thiosemicarbazone Me_2NNMe_2 induces paraptosis by disrupting the ER thiol redox homeostasis based on protein disulfide isomerase inhibition. *Cell Death Dis.* **2018**, *9*, 1052. doi:10.1038/s41419-018-1102-z

[56] Lee, E.; Lee, D. H. Emerging roles of protein disulfide isomerase in cancer, *BMB Rep.* **2017**, *50*, 401-410. DOI: 10.5483/bmbrep.2017.50.8.107

[57] Sîrbu, A.; Palamarciuc, O.; Babak, M. V.; Lim, J. M.; Ohui, K.; Enyedy, E. A.; Shova, S.; Darvasiová, D.; Rapta, P.; Ang, W. H.; Arion, V. B. Copper(II) thiosemicarbazone complexes induce marked ROS accumulation and promote nrf2-mediated antioxidant response in highly resistant breast cancer cells. *Dalton Trans.* **2017**, *46*, 3833-3847. DOI:10.1039/C7DT00283A

[58] Zeglis, B. M.; Divilov, V.; Lewis, J. S. Role of Metalation in the Topoisomerase IIα Inhibition and Antiproliferation Activity of a Series of r-Heterocyclic-N4-Substituted Thiosemicarbazones and Their Cu(II) Complexes. *J. Med. Chem.* **2011**, *54*, 2391-2398. DOI: 10.1021/jm101532u

[59] Rogolino, D.; Bacchi, A.; De Luca, L.; Rispoli, G.; Sechi, M.; Stevaert, A.; Naesens, L.; Carcelli, M. Investigation of the salicylaldehyde thiosemicarbazone scaffold for inhibition of influenza virus PA endonuclease. *J. Biol. Inorg. Chem.*, **2015**, *20*, 1109-1121. DOI: 10.1007/s00775-015-1292-0

[60] Fisicaro, E.; Braibanti, A. *Talanta* **1988**, *35*, 769-774. DOI: 10.1016/0039-9140(88)80181-4

(61] Tegoni, M.; Furlotti, M.; Tropiano, M.; Lim, C. S.; Pecoraro, V. L. *Inorg. Chem.* **2010**, *49*, 5190-201. DOI: 10.1021/ic100315u

[62] Vogel, A. I. Quantitative Inorganic Analysis Including Elementary Instrumental Analysis, **1962,** Longmans, London, UK, Third ed.

[63] Gans, P.; Sabatini, A.; Vacca, A. Investigation of equilibria in solution. Determination of equilibrium constants with the HYPERQUAD suite of programs. *Talanta*, **1996**, *43*, 1739-1753. DOI: 10.1016/0039-9140(96)01958-3

[64] Gans, P.; Sabatini, A.; Vacca, A. Determination of equilibrium constants from spectrophometric data obtainedfrom solutions of known pH: The program pHab. *Annali di Chimica*, **1999**, *89*, 45-49.

[65] Alderighi, L.; Gans, P.; Ienco, A.; Peters, D.; Sabatini, A.; Vacca, A. Hyperquad simulation and speciation (HySS): A utility program for the investigation of equilibria involving soluble and partially soluble species. *Coord. Chem. Rev.* **1999**, *184*, 311-318. DOI:10.1016/S0010 8545(98)00260-4

[66] SAINT: SAX, Area Detector Integration, Siemens Analytical Instruments Inc., Madison, Wisconsin, USA

[67] Sheldrick, G. SADABS: Siemens Area Detector Absorption Correction Software, University of Goettingen, Germany, 1996.

[68] Altomare, A.; Burla, C.; Camalli, M.; Cascarano, G.L.; Giacovazzo, C.; Guagliardi, A.; Moliterni, A.G.G.; Polidori, G.; Spagna, R. *J. Appl. Crystallogr*. **1999**, *32*, 115-119.

[69] Sheldrick, G.M. A short history of SHELX. *Acta Cryst.* **2008**, A64, 112-122. DOI: 10.1107/S0108767307043930

[70] Farrugia, L.J. WinGX suite for small-molecule single-crystal crystallography. *J. Appl. Crystallogr.* **1999**, *32*, 837-838. DOI: 10.1107/S0021889899006020

[71] Gandin, V.; Pellei, M.; Tisato, F.; Porchia, M.; Santini, C.; Marzano, C. A novel copper complex induces paraptosis in colon cancer cells via the activation of ER stress signalling, *J. Cell. Mol. Med.* **2012**, *16*, 142-151. DOI: 10.1111/j.1582-4934.2011.01292.x.

[72] Alley, M.C.; Scudiero, D.A.; Monks, A.; Hursey, M.L.; Czerwinski, M.J.; Fine, D.L.; Abbott, B.J.; Mayo, J.G.; Shoemaker, R.H.; Boyd, M.R. Feasibility of drug screening with panels of human tumor cell lines using a microculture tetrazolium assay. *Cancer. Res.* **1988**, *48*, 589-601.

[73] Gandin, V.; Ceresa, C.; Esposito, G.; Indraccolo, S.; Porchia, M.; Tisato, F.; Santini, C.; Pellei, M.; Marzano, C. Therapeutic potential of the phosphino Cu(I) complex (HydroCuP) in the treatment of solid tumors. *Sci. Rep.* **2017**, *7*, 13936. DOI: 10.1038/s41598-017-13698-1

[74] Rigobello, M.P.; Gandin, V.; Folda, A.; Rundloef, A.-K.; Fernandes, A.P.; Bindoli, A.; Marzano, C.; Bjoernstedt, M. Treatment of human cancer cells with selenite or tellurite in combination with auranofin enhances cell death due to redox shift. *Free Radic. Biol. Med.*, **2009,** *47*, 710-721. DOI: 10.1016/j.freeradbiomed.2009.05.027

[75] Bindoli, A.; Callegaro, M. T.; Barzon, E.; Benetti, M.; Rigobello, M. P. Influence of the redox state of pyridine nucleotides on mithocondrial sulfhydryl groups and permeability transition. *Arch. Biochem. Biophys.*, **1997**, *342*, 22-28.

Table of Content Graphic

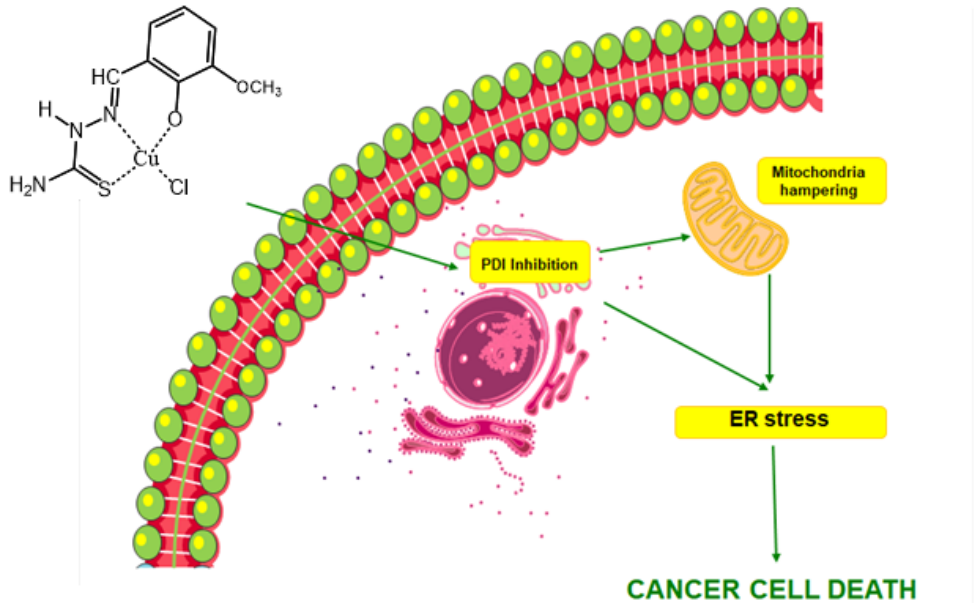

IC_{50} (mM) ± S.D.		
HCT-15	PSN-1	A375
0.004±0.001	0.008±0.002	0.003±0.004